A Unified Algorithm for Phase-Stability/ Split Calculation for Multiphase Isobaric-Isothermal Flash

Di Zhu, University of Texas at Austin; **Sara Eghbali,** University of Alberta; and **Chandra Shekhar** and **Ryosuke Okuno,** University of Texas at Austin

Summary

The conventional method for multiphase flash is the sequential usage of phase-stability and phase-split calculations. Multiphase flash requires the conventional method to obtain multiple false solutions in phase-split calculations and correct them in phase-stability analysis. Improvement of the robustness and efficiency of multiphase flash is important for compositional flow simulation with complex phase behavior.

This paper presents a new algorithm that solves for stationary points of the tangent-plane-distance (TPD) function defined at an equilibrium-phase composition for isobaric-isothermal (PT) flash. A solution from the new algorithm consists of two groups of stationary points: tangent and nontangent stationary points of the TPD function. Hence, equilibrium phases, at which the Gibbs free energy is tangent to the TPD function, are found as a subset of the solution.

Unlike the conventional method, the new algorithm does not require finding false solutions for robust multiphase flash. The advantage of the new algorithm in terms of robustness is more pronounced for more-complex phase behavior, for which multiple local minima of the Gibbs free energy are present. Case studies show that the new algorithm converges to a lower Gibbs free energy compared with the conventional method for the complex fluids tested. It is straightforward to implement the algorithm because of the simple formulation, which also allows for an arbitrary number of iterative compositions. It can be robustly initialized even when no K value correlation is available for the fluid of interest. Although the main focus of this paper is on robust solution of multiphase flash, the new algorithm can be used to initialize a second-order convergent method in the vicinity of a solution.

Introduction

A multiphase equilibrium calculation for a fixed pressure (P) and temperature (T) requires global minimization of the Gibbs free energy subject to material balance. The conventional algorithms after Michelsen (1982a, b) are based on the sequential usage of phase-stability and -split calculations. That is, a phase-stability calculation is performed for the overall composition specified or one of the phases from a multiphase solution, at which the plane tangent to the Gibbs free energy surface is defined. If it detects phase instability, a phase-split calculation is performed under the assumption that one more equilibrium phase is present.

For instance, calculation for three equilibrium phases starts with testing the stability for the overall composition specified. Once phase instability is detected, a two-phase-split calculation is conducted for the overall composition. Then, phase stability is tested for one of the two phases obtained from the two-phase flash. After detecting the instability of the two-phase solution, a three-phase-split calculation is performed. Finally, one of the three phases is used to test the stability of the three-phase solution.

There are many algorithms presented in the literature for each of the phase-stability and -split calculations for an assumed number of phases. Successive substitution is the classical algorithm used for each of the phase-stability and -split calculations. It is linearly convergent for nonideal mixtures, but known to be reliable (Mehra et al. 1983; Ammar and Renon 1987; Kaul 1992; Pan and Firoozabadi 2003; Michelsen and Mollerup 2004). Therefore, it is commonly used to provide an initial estimate for higher-order methods to achieve the final convergence (Mehra et al. 1982; Michelsen 1982b; Nghiem et al. 1983; Ammar and Renon 1987; Pan and Firoozabadi 2003).

Various algorithms were developed and compared for phase-split calculations for an assumed number of phases and phase-stability testing (Gautam and Seider 1979; Ohanomah and Thompson 1984; Lucia et al. 1985; Trangenstein 1985, 1987; Ammar and Renon 1987; Litvak 1994; Teh and Rangaiah 2002), such as interval methods (Hua et al. 1996, 1998a, b; Xu et al. 2000; Tessier et al. 2000; Xu et al. 2002; Burgos-Solórzano et al. 2004; Xu et al. 2005) and trust-region methods (Nghiem et al. 1983; Lucia and Liu 1998; Lucia and Yang 2003; Lucia et al. 2012). A widely used algorithm is minimization of the Gibbs free energy by use of Newton's method with a line-search technique, in which the modified Cholesky decomposition of Gill and Murray (1974) is used to provide a search direction when the Hessian matrix is not positive-definite (Michelsen 1982a, b; Perschke et al. 1989). A popular quasi-Newton method is the Broyden-Fletcher-Goldfarb-Shanno method (Broyden 1970a, b; Fletcher 1970; Goldfarb 1970, 1976; Shanno 1970; Lucia et al. 2000) for an inverse of the Hessian matrix approximation. Lucia and Macchietto (1983) and Venkataraman and Lucia (1986, 1987) developed a thermodynamically consistent quasi-Newton method on the basis of Lucia and Macchietto (1983).

The sequential use of phase-stability and -split calculations has been successfully applied for various compositional flow problems in the literature (e.g., Mehra et al. 1983; Nghiem and Li 1984; Perschke 1988; Han and Rangaiah 1998), and is called the conventional approach in this paper. However, it is a series of local solutions for assumed numbers of phases, which requires obtaining and correcting false solutions for multiphase problems. Correction of false solutions in phase-stability analysis is highly sensitive to the initial guess used for the search for potential equilibrium phases. Also, it is not always possible to obtain a reasonable set of initial K values for multiphase reservoir fluids.

For example, three different types of two equilibrium phases (L_1+V, L_1+L_2, and L_2+V) exist in composition space that contains three equilibrium phases (L_1+L_2+V), where L_1, L_2, and V stand for the oleic, solvent-rich liquid, and gaseous phases, respectively. When L_1+L_2 or L_2+V is of the global minimum in the Gibbs free energy at the specified flash conditions, the conventional algorithms started with Wilson's correlation (Wilson 1969) often fail to converge to the correct solution, or tend to be attracted by local minima before reaching it through negative flash (see Case 4 in this paper). However, no method has been established to estimate K values for a hydrocarbon mixture involving the L_2 phase.

This paper (SPE 175060) was accepted for presentation at the SPE Annual Technical Conference and Exhibition, Houston, 28–30 September 2015, and revised for publication. Original manuscript received for review 22 June 2016. Revised manuscript received for review 11 July 2017. Paper peer approved 13 July 2017.

One way to improve the robustness of multiphase flash is to use multiple initial guesses in a series of phase-stability analyses, as given in Michelsen (1982b), Perschke (1988), and Li and Firoozabadi (2012). However, it still requires obtaining and correcting false solutions, which are often near local minima of the Gibbs free energy subject to material balance. As will be shown in this paper, many stability calculations with different initial K values may be required to obtain merely a false solution in multiphase flash.

Gupta et al. (1991) presented a novel methodology to perform phase-stability and -split calculations simultaneously. In their algorithm, the Rachford-Rice (RR) and stability equations were solved simultaneously for phase amounts and "stability variables" by use of Newton's method for root finding. The stability equations of Gupta et al. (1991) indicate that either the stability variable or the phase amount of an individual phase is zero at the global minimum of the Gibbs free energy. The stability variables of Gupta et al. (1991) were derived from the first-order condition for unconstrained minimization of the Gibbs free energy as formulated by them. K values were then updated in the outer loop by successive substitution. Unlike conventional successive substitution, however, the flash algorithm of Gupta et al. (1991) involves the simultaneous root-finding of the RR and stability equations, which can cause convergence issues, as discussed below.

Various issues with the Gupta et al. (1991) algorithm were reported in previous papers, and have also been identified in the current research. First, researchers (Abdel-Ghani 1995; Alsaifi and Englezos 2011) reported numerical issues associated with the degeneracy of equations (called "stability equations" in their papers) near phase boundaries on the basis of the Gupta et al. (1991) formulation. Second, the initialization scheme they proposed often results in K values that give an unbounded feasible region for the RR solution. As proved in Okuno et al. (2010a), such an RR problem has no solution, which stops the flash calculation from proceeding. Even if it is successfully initialized, the original algorithm of Gupta et al. (1991) may not be robust because it does not check the feasibility of each RR solution during the iteration. Third, it is not clear how their algorithm selects the reference composition that is required to set the system of equations to be solved. It is likely that negative phase amounts are used as the indicator for improper selection of the reference composition, as mentioned in Alsaifi and Englezos (2011).

Alsaifi and Englezos (2011) used the trust-region-Gauss-Newton method with the original formulation of Gupta et al. (1991). It was reported that, unlike the algorithm of Gupta et al. (1991), their algorithm did not encounter convergence issues near phase boundaries. However, no comparison was given between the two algorithms. It is not entirely clear how the reported improvement was achieved. The algorithm developed by us in this research does not require the equations [called "stability equations" in Gupta et al. (1991)] that caused the convergence issues near phase boundaries.

Chaikunchuensakun et al. (2002) also proposed a simultaneous solution of phase-stability and -split calculations on the basis of minimization of the Gibbs free energy. They used a quasi-Newton method with an approximate Hessian matrix rather than an analytical one. Use of pseudocritical properties of the fluid of interest was proposed for identification of the states of the reference and potential equilibrium phases. If the ratio of the system pressure to the pseudocritical pressure of the fluid is greater than a value that is heuristically determined (e.g., 1.0, as used in their paper), the fluid is identified as a liquid; otherwise, the mixture is a vapor. However, Chaikunchuensakun et al. (2002) stated that their algorithm is only for local minimization, and does not attempt to search for a global solution for multiphase PT flash. Also, it is not clear why the phase identification is required in their algorithm.

This paper presents the correct set of equations and constraints that can be easily solved for simultaneous phase-stability and -split calculations for PT multiphase flash. The formulation does not require the stability equations that the algorithm of Gupta et al. (1991) and its variants (Abdel-Ghani 1995; Chaikunchuensakun et al. 2002; Alsaifi and Englezos 2011) used. The main novelty of our work is in the unified use of the TPD function (Baker et al. 1982; Michelsen 1982a) for PT multiphase flash for an arbitrary number of iterative compositions. It allows for flexibility in terms of the amount of information regarding the Gibbs free energy used during the iterative solution by controlling the number of iterative compositions initialized. A new algorithm is developed on the basis of successive substitution augmented with some important steps for global convergence for the formulated PT multiphase flash. Case studies are given to demonstrate the robustness of the developed algorithm.

Algorithm

Global minimization of the Gibbs free energy in composition space for PT flash is formulated such that all stationary points of the TPD function defined at the overall composition specified or one of the equilibrium phases must be nonnegative. This is a direct representation of the classical criterion for phase equilibrium, as explained in Baker et al. (1982). As shown in the formulation presented in Appendix A, the TPD function is used in a unified manner for all stationary points of the TPD at an equilibrium state, which consist of tangent stationary points (i.e., equilibrium phase compositions with zero TPD) and the other stationary points (i.e., compositions with positive TPD values). That is, equilibrium phases are considered as a subset of TPD stationary points in the new formulation (Appendix A). Then, multiphase PT flash is used to find a plane tangent to the Gibbs free energy such that it does not lie above the Gibbs free energy at all stationary points identified. In what follows, we first show working equations and then a stepwise description of the algorithm. The corresponding flow chart is given in Appendix B.

The algorithm developed to solve the formulated problem (Appendix A) does not require the number of equilibrium phases to be set before the iteration. It aims to find stationary points of the TPD function defined at one of the equilibrium phases upon convergence. Iterative compositions are distributed in composition space in the initialization step, and they search for stationary points along the search directions determined by traditional successive substitution. That is, the algorithm uses the TPD equation

$$f_{ij} = \ln(x_{ij}\varphi_{ij}) - \ln(x_{ir}\varphi_{ir}) - \theta_j = 0 \quad (1)$$

to update all iterative compositions $x_{ij} (i = 1, 2, \ldots, N_C$ and $j = 1, 2, \ldots, N_S)$ through K values by use of successive substitution. In Eq. 1, N_C is the number of components and N_S is the number of iterative "sampling" compositions that capture thermodynamic information in composition space during the iteration. The fugacity coefficient of component i at sampling composition j is denoted as φ_{ij}.

It is important to note that the equations and variables used in the algorithm given in this section correspond to those in the formulation (Appendix A) only upon convergence, because the formulation is based on an equilibrium state. For example, $\theta_j = D_{Rj}$ (Eq. A-14) at an equilibrium state upon convergence. The number of iterative sampling compositions becomes the number of stationary points upon convergence, but both are denoted as N_S in this paper. The reference composition x_{ir} $(i = 1, 2, \ldots, N_C)$ is one of the sampling compositions during the iteration, and becomes one of the tangent stationary points upon convergence.

As stated in Appendix A, N_P equilibrium phases satisfy $D_{Rj} = 0$ along with Eqs. A-2, A-3, and A-4 for $j = 1, 2, \ldots, N_P$. The other N_U stationary points satisfy $D_{Rj} > 0$ and Eq. A-4 for $j = (N_P+1), (N_P+2)\ldots, N_S,$ where $N_S = N_P + N_U$. During the iteration, N_S sampling compositions belong to either set P or U. In set P, $\theta_j = 0$ and $\beta_j > 0$ for $j = 1, 2, \ldots, N_P$. In set U, $\theta_j > 0$ and $\beta_j = 0$ for $j = (N_P+1), (N_P+2)\ldots, N_S$. Upon convergence, the sampling compositions in set P correspond to equilibrium phases, and sampling compositions in set U

correspond to stationary points of the converged TPD function, at which D_R values are positive. In other words, the converged sampling compositions in set P are tangent stationary points and those in set U are nontangent stationary points.

Successive substitution is performed to solve Eq. 1 together with Eqs. A-2, A-3, and A-4 for K values, which are defined as

$$K_{ij} = x_{ij}/(e^{\theta_j} x_{ir}) \quad \ldots\ldots (2)$$

for $i = 1, 2, \ldots, N_C$, and $j = 1, 2, \ldots, N_S$, except for the reference, r. The reference composition $\underline{x}_r$ is selected from set P adaptively, as described later.

For set P, Eq. 2 becomes $K_{ij} = x_{ij}/x_{ir}$. The conventional RR equations give the relationship between K values and mole fractions of apparent phases (β_j) as follows:

$$g_j = \sum_{i=1}^{N_C}(x_{ir} - x_{ij}) = \sum_{i=1}^{N_C}(1 - K_{ij})z_i/t_i = 0 \quad \ldots\ldots (3)$$

for sampling point $j \neq r$ within set P, where $t_i = 1 - \sum_{k=1,k\neq r}^{N_P}(1 - K_{ik})\beta_k$ for $i = 1, 2, \ldots, N_C$. Compositions are given as $x_{ir} = z_i/t_i$ and $x_{ij} = K_{ij}x_{ir}$ for sampling point $j \neq r$.

For set U, the summation constraint $\Sigma_i x_{ij} = 1.0$ gives

$$\theta_j = -\ln\left[\sum_{i=1}^{N_C} K_{ij}x_{ir}\right] \quad \ldots\ldots (4)$$

for sampling composition j within set U. Compositions for set U are given as $x_{ij} = e^{\theta_j}K_{ij}x_{ir}$ for $i = 1, 2, \ldots, N_C$.

The fundamental structure of the current algorithm broadly follows the traditional successive substitution algorithm, but phase-stability and -split calculations are performed in an integrated manner. That is, each iteration first solves Eq. 3 for compositions for set P for a given set of K values and overall composition. Then, Eq. 4 is used to obtain compositions for set U for a given set of K values and reference composition. After that, K values are updated for sets P and U by use of Eqs. 1 and 2:

$$\ln K_{ij} = \ln\varphi_{ir} - \ln\varphi_{ij}. \quad \ldots\ldots (5)$$

One of the most important factors that affect global convergence of the algorithm is how iterative sampling compositions are distributed in composition space (e.g., the number of initial sampling compositions and their locations). Sampling compositions can be initialized by use of a correlation suitable for the fluid of interest, such as Wilson's correlation, Li and Firoozabadi (2012), and Zhu and Okuno (2015, 2016); or use of certain information from the previous timestep in flow simulation; or use of tie-simplex information in composition space (Iranshahr et al. 2010); or a systematic distribution in composition space if no reliable information is available regarding equilibrium phase compositions. Ideally, they are supposed to converge to all stationary points of TPD so that the global minimum of the Gibbs free energy is ensured upon convergence. Such a possibility is generally expected to increase as more sampling compositions are used, unless they are placed close to each other. As an example for the fourth type of initialization, Appendix C describes the initialization method used in the case studies in this paper, which systematically distribute sampling compositions in composition space. Obviously, there are many other distributions that are equally applicable for engineering applications.

In general, flash calculation is more efficient when it is initialized with certain reliable information available for expected equilibrium phases. In case studies in this research, the fourth type of initialization is used because they are all standalone multiphase flash. In one of the case studies, however, the new algorithm is tested with Wilson's correlation, and is shown to efficiently find a lower Gibbs free energy than the conventional sequential method.

Other important steps for enhanced robustness include the feasibility check for each RR solution by use of the method of Okuno et al. (2010a). The constraint, $a_i^T\boldsymbol{\beta} \leq b_i$, where $a_i = \{1–K_{ij}\}$, $\boldsymbol{\beta} = \{\beta_j\}$, $b_i = \min\{1–z_i, \min_j\{1–K_{ij}z_i\}\}$ for $i = 1, 2, \ldots, N_C$, is to be satisfied for compositions in set P if there exists a bounded feasible region for each RR solution, as described in Okuno et al. (2010a). Also, the constraints regarding β_j and θ_j described previously are used for classification of sampling compositions for sets P and U during the iteration.

The Peng and Robinson (PR) equation of state (EOS) (Peng and Robinson 1976, 1978) with the van der Waals mixing rules is used to calculate thermodynamic properties in this research. A stepwise description of the algorithm used in this paper is given here.

Step 1. Set N_S sampling compositions $\underline{x}_j^{(k)}$ for $j = 1, 2, \ldots, N_S$. The number in the parentheses represents the iteration step number; $k = 1$ for the initial step.

Step 2. Calculate D_{Rj} for $j = 1, 2, \ldots, N_S$ with $\underline{z}_i$ as the reference composition by use of Eq. A-13. Select the sampling composition with the minimum D_R value as the reference composition, $\underline{x}_r^{(1)}$. Calculate K values, $\underline{K}_j^{(1)}$, by use of $\ln K_{ij} = \ln\varphi_{ir} - \ln\varphi_{ij}$ for $i = 1, 2, \ldots, N_C$ and $j = 1, 2, \ldots, N_S$ except for r. Recalculate D_{Rj} with $\underline{x}_r^{(1)}$, and set N_U as the number of sampling compositions with positive D values. $N_P = N_S–N_U$. If $N_P > 1$, continue to Step 3.

If $N_P = 1$, select $\underline{z}$ as $\underline{x}_r^{(1)}$. This increases N_S by one because $\underline{z}$ becomes part of the sampling compositions. Calculate $\underline{K}_j^{(1)}$, D_{Rj}, N_U, and N_P as described previously. If $N_P = 1$, go to Step 6; otherwise, go to Step 3.

Step 3. Check the feasibility of the RR solution for set P by use of the method of Okuno et al. (2010a). If feasible, go to Step 5. Otherwise, continue to Step 4.

Step 4. Exclude from set P as many sampling compositions as required until the feasibility is satisfied for the given RR problem. Update N_P. $N_U = N_S–N_P$. If $N_P = 1$, go to Step 6. Otherwise, continue to Step 5.

Step 5. Perform the convex minimization to obtain $\underline{x}_j^{(k)}$ and $\beta_j^{(k)}$ for set P that satisfy Eq. 3, as presented in Okuno et al. (2010a). The convergence criterion is that $\|g_j\|_\infty < \varepsilon_g$. $\varepsilon_g = 10^{-10}$ is used in this research, but it can be a larger number for practical applications.

Step 6. Obtain $\underline{x}_j^{(k)}$ and $\theta_j^{(k)}$ for set U by use of Eq. 4.

Step 7. Check to determine whether there is any $\theta_j^{(k)}$ that is negative in set U. If so, select the sampling composition that has the minimum θ_j value as $\vec{x}_r$, and update N_U. $N_P = N_S–N_U$. Go to Step 10. Otherwise, continue to Step 8.

Step 8. Check to determine whether there is any $\beta_j^{(k)}$ that is negative in set P. If so, select the sampling composition with $0 < \beta_j < 1$ as $\underline{x}_r$ and update N_U. $N_P = N_S–N_U$. Go to Step 10. Otherwise, continue to Step 9.

Step 9. Check for convergence. Stop if $\|f_{ij}\|_\infty < \varepsilon_f$. In this research, $\varepsilon_f = 10^{-10}$ is used, but it can be a larger number for practical applications. Otherwise, continue to Step 10.

Step 10. Check to determine whether there are any compositions to be merged on the basis of the criterion that the maximum norm for two compositions is less than ε_x (e.g., $\varepsilon_x = 10^{-3}$). If so, perform necessary updates for N_S and N_U. $N_P = N_S - N_U$.

Step 11. Update K values by use of Eqs. 1 and 2; i.e., $\ln K_{ij}^{(k+1)} = \ln\varphi_{ir}^{(k)} - \ln\varphi_{ij}^{(k)}$ for $i = 1, 2, \ldots, N_C$ and $j \neq r$. Increase the iteration step index by one; $k = k + 1$. Go to Step 6 if $N_P = 1$. Otherwise, go to Step 3.

Steps 1, 5, 9, and 10 require user-specified values. The procedure presented in Appendix C is used for Step 1 in this paper. However, it can be replaced by other procedures, such as correlations for the fluid under consideration, the flash solution from the previous timestep in flow simulation, and use of a random-number generator. Steps 5 and 9 require convergence criteria, and Step 10 requires a merging criterion.

Step 2 sets the reference composition that is required to define Eq. 1 in the initialization. First, TPD is calculated by function D_R (Eq. A-13) at N_S sampling compositions with the overall composition $\underline{z}$ as the reference composition $\underline{x}_r$. Then, the initial reference composition is redefined that gives the minimum D_R among the N_S sampling compositions. Note that Eq. A-14 cannot be used for this initialization step because the N_S initial sampling compositions are not stationary points of TPD defined at $\underline{z}$. Steps 7 and 8 describe how to update a reference composition when the constraints regarding β_j and θ_j are not satisfied during the iteration.

In Step 4, the exclusion of sampling compositions from set P is performed depending on their D_{Rj} values from Eq. A-13. That is, the sampling composition with the largest D_{Rj} value among set P is first excluded. The subsequent exclusions, if necessary, are in the order of decreasing D_R. If Step 4 is taken in the first iteration ($k = 1$), the D_{Rj} values calculated in Step 2 are directly used.

In Step 5, it is crucial to precisely implement the multiphase RR algorithm as described in Okuno et al. (2010a). In particular, it is recommended to confirm the following for each RR solution:

- The feasible region for β_j ($j = 1, 2, \ldots, N_P$) should be based on nonnegativity of components' mole fractions, $0 \leq x_{ij} \leq 1$ ($i = 1, 2, \ldots, N_C$, and $j = 1, 2, \ldots, N_P$). Note that the function to be minimized in the RR solution is nonmonotonic and convex within its feasible region (Michelsen 1994; Michelsen and Mollerup 2004; Okuno et al. 2010a).
- The initial values for β_j ($j = 1, 2, \ldots, N_P$) should be placed inside the feasible region.
- Under-relaxation should be performed if a Newton step is found to bring the iterate to the infeasible domain, to keep β_j ($j = 1, 2, \ldots, N_P$) feasible. It is straightforward to calculate the maximum step size to be taken to reach a feasibility limit along a given search direction (Newton's direction) because the feasibility limits are all linear [Eq. 10 in Okuno et al. (2010a)].

The new algorithm is to locate stationary points of TPD that give the global minimum of the Gibbs free energy at the specified T and P with the well-known convergence behavior of successive substitution (Mehra et al. 1983; Ammar and Renon 1987; Kaul 1992). Michelsen (1982a) showed that successive substitution for the stationary-point method of phase-stability analysis converges to a minimum, instead of a maximum or saddle point, of the TPD function. It has been observed in this research that the developed algorithm also converges to minima of the TPD function.

In the new algorithm, equilibrium phases are found as a subset of the converged stationary points; that is, the number of phases is part of the solution. One of the main differences from the conventional flash is that the unified TPD equations (Eq. 1) can be solved with an arbitrary number of sampling compositions. This gives the flexibility in terms of robustness and efficiency that the algorithm offers; e.g., use of more sampling compositions increases the level of robustness at the expense of the increased number of equations, at least for the initial stage of iteration. As will be discussed later, extra sampling compositions naturally merge for a case in which N_S is greater than the number of stationary points present upon convergence.

The algorithm presented previously is substantially different from that of Gupta et al. (1991). An important difference comes from the difference in formulation; that is, they introduced an additional set of equations, $\beta_j\theta_j = 0$, which were called "stability equations" in their papers. A similar set of equations, $\beta_j\theta_j/(\beta_j+\theta_j) = 0$, were then solved simultaneously with the RR equations in their algorithm. However, Appendix A clearly shows that the complete formulation does not require the stability equations of Gupta et al. (1991). The correct set of equations in the current paper does not have the degeneracy issues that the algorithm of Gupta et al. (1991) exhibits near phase boundaries because of their stability equations, as reported by Alsaifi and Englezos (2011).

The robustness of the current algorithm also comes from the careful initialization (Step 1) and adaptive selection of the reference composition (Steps 2, 7, and 8). The initialization scheme of Gupta (1990) eliminates the sampling compositions that have positive D values from Eq. A-13 with $\underline{z}$ as the reference composition. However, this often leads to a complete failure of the calculation.

The simplicity of the formulation has led to the straightforward iteration steps, which are essentially the widely used successive substitution. Unlike other related publications after Gupta et al. (1991), such as Abdel-Ghani (1995), Chaikunchuensakun et al. (2002), and Alsaifi and Englezos (2011), the robust solution of multiphase RR equations (Okuno et al. 2010a) further enhances the robustness of the current algorithm.

Case Studies

The new algorithm can make multiphase flash problems straightforward by not having to solve for false solutions and correct them. This section presents case studies to demonstrate the robustness and simplicity of the new algorithm with the initialization method presented in Appendix C. All case studies presented in this section are performed with the in-house software developed by Zhu et al. (2017). The convergence criteria used for the new algorithm are stated previously (e.g., $\varepsilon_f = \varepsilon_g = 10^{-10}$ and $\varepsilon_x = 10^{-3}$).

The new algorithm is compared with the conventional method of sequential phase-stability and -split calculations and the method of Gupta et al. (1991). In the sequential method used for this section, single-phase stability analysis is performed with two initial guesses, searching for a V-like phase first and an L-like phase next, on the basis of Wilson's K values (Michelsen 1982a). For stability analysis for multiple phases, initial guesses recommended by Firoozabadi (1999) and Li and Firoozabadi (2012) are used in addition to the V-like and L-like guesses, in the following order: a V-like phase, an L-like phase, compositions near vertices in composition space, the midpoint of phase compositions, and $\varphi_i x_i$ for $i = 1, 2, \ldots, N_C$.

Calculations in this section use only successive substitution for a fair comparison in terms of robustness. However, the new algorithm based on successive substitution can be switched to any second-order convergent method in the vicinity of a solution, when the residual of Eq. 1 becomes less than a certain criterion, as will be shown for Case 4. Direct application of Newton's method for the formulated problem (Appendix A) is to be investigated. The iteration scheme used for the new algorithm is essentially the traditional successive substitution. As presented in Heidemann and Michelsen (1995), successive substitution may not converge if negative binary interaction parameters are used for attraction terms in a cubic-EOS fluid model.

The convergence criterion used for stability analysis in the conventional method is that the maximum norm of stationarity equations is less than 10^{-10}. The convergence criterion used for phase-split calculations in the conventional method is that the maximum norm of fugacity equations is less than 10^{-10}. Use of 10^{-10} for these convergence criteria is equivalent to the use of $\varepsilon_f = 10^{-10}$ for the new algorithm. The criterion used for a trivial solution in the conventional stability analysis is 10^{-3}, which is equivalent to the merging criterion $\varepsilon_x = 10^{-3}$ in the new algorithm.

The number of fugacity-coefficient calculations is reported as a measure of computational cost, in addition to the number of iterations required for convergence, for each case. Both metrics depend on the initial N_S and their locations with the new algorithm; i.e., results regarding the computational cost will be different if other initialization methods are used. A calculation for a vector consisting of $\ln\varphi_i$ for $i = 1, 2,\ldots, N_C$ is counted as one.

Case 1. This case uses mixtures of H_2O, C_3, and n-C_{16} to graphically show a few important features of the new algorithm. The properties used for the components are given in **Table 1. Fig. 1** shows the two- and three-phase regions in composition space at 430 K and 35 bar for the ternary system. In Fig. 1, *L, V,* and *W* represent the oleic, gaseous, and aqueous phases, respectively.

Component	T_C (K)	P_C (bar)	ω
H_2O	647.3000	220.8900	0.3440
C_3	369.8000	42.4600	0.1520
n-C_{16}	717.0000	14.1900	0.7420
Binary Interaction Parameters			
	H_2O	C_3	n-C_{16}
H_2O	0.0000	0.6841	0.3583
C_3	–	0.0000	0.0000
n-C_{16}	–	–	0.0000

Table 1—Properties of the components for Case 1.

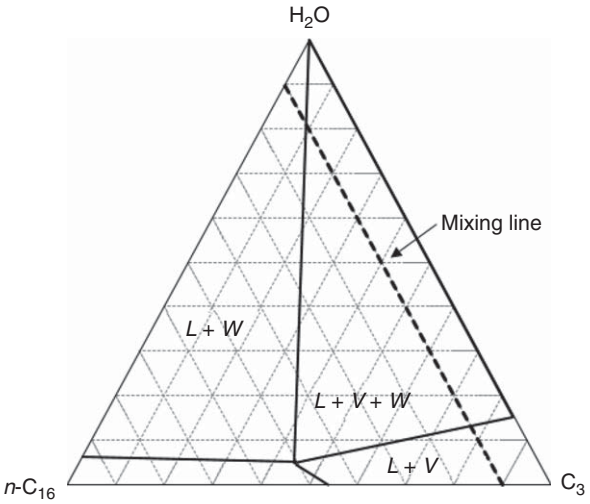

Fig. 1—Phase boundaries for the ternary system of H_2O, C_3, and n-C_{16} at 430 K and 35 bar. *L, V,* and *W* stand for the oleic, gaseous, and aqueous phases, respectively. Properties of the components are given in Table 1. The mixing line between (0.0, 0.9, 0.1) and (0.9, 0.0, 0.1) is used to show the variation of parameters in Figs. 2 and 3.

The new algorithm is applied with initial $N_S = 6$ along the mixing line between (0.0, 0.9, 0.1) and (0.9, 0.0, 0.1). Out of the six sampling compositions, three compositions are placed near the compositional vertices, and the others are the central points in the three regions surrounding a given overall composition (R_i for $i = 1$, 2, and 3, as given in Appendix C). The six sampling compositions initially distributed merge into three stationary points that correspond to the *L, V,* and *W* phases on the Gibbs free energy surface. **Fig. 2** shows the Gibbs free energy surface at 430 K and 35 bar, and the tangent planes converged for three overall compositions with H_2O concentrations of 0.10, 0.75, and 0.84 along the mixing line. It has been visually confirmed that the algorithm has successfully converged to the global minimum of the Gibbs free energy subject to material balance for each overall composition.

Fig. 3 shows the behavior of the converged β_j and θ_j along the mixing line. One nontangent stationary point in set U is observed in the two-phase regions ($L + V$ and $L + W$) along the mixing line. The D_R values at such nontangent stationary points in Fig. 2 can be confirmed with Fig. 3b; e.g., θ_W of 0.2478 for $z_{H_2O} = 0.1$. They qualitatively indicate how close the current equilibrium state is to a phase transition, as can be seen in Fig. 3b. Hence, the new algorithm provides more global information about the Gibbs free energy than the conventional sequential method, when it converges to nontangent stationary points with positive D_R values.

Figs. 1, 2, and 3 present that different sets of equilibrium phases can be easily calculated as thermodynamically stable stationary points by use of the unified algorithm that directly converges to the correct solution. Unlike the current algorithm, the negative flash approach (Whitson and Michelsen 1989) may indicate phase instability with negative β values when obtaining a false solution.

The new algorithm is compared with the method of Gupta et al. (1991) by use of the overall composition of 75% H_2O, 15% C_3, and 10% n-C_{16} at 560 K and 65 bar. The critical endpoint of type $L_1 = V + W$ is calculated for this mixture at 569.35 K and 130.07 bar by use of the PR EOS. The correct solution of L_1+V is given in **Table 2.** The method of Gupta et al. (1991) cannot converge to this solution for several reasons. First, the initialization scheme proposed by Gupta (1990) yields an RR problem with an unbounded feasible domain, resulting in a failure in initialization. Second, even when initialized successfully with the method given in Appendix C (e.g., $N_S = 6$), their algorithm stops proceeding at the 10th iteration step because of an open feasible domain encountered for the RR solution. These types of failures occur for the next cases with the algorithm of Gupta et al. (1991), although they are not presented in this paper.

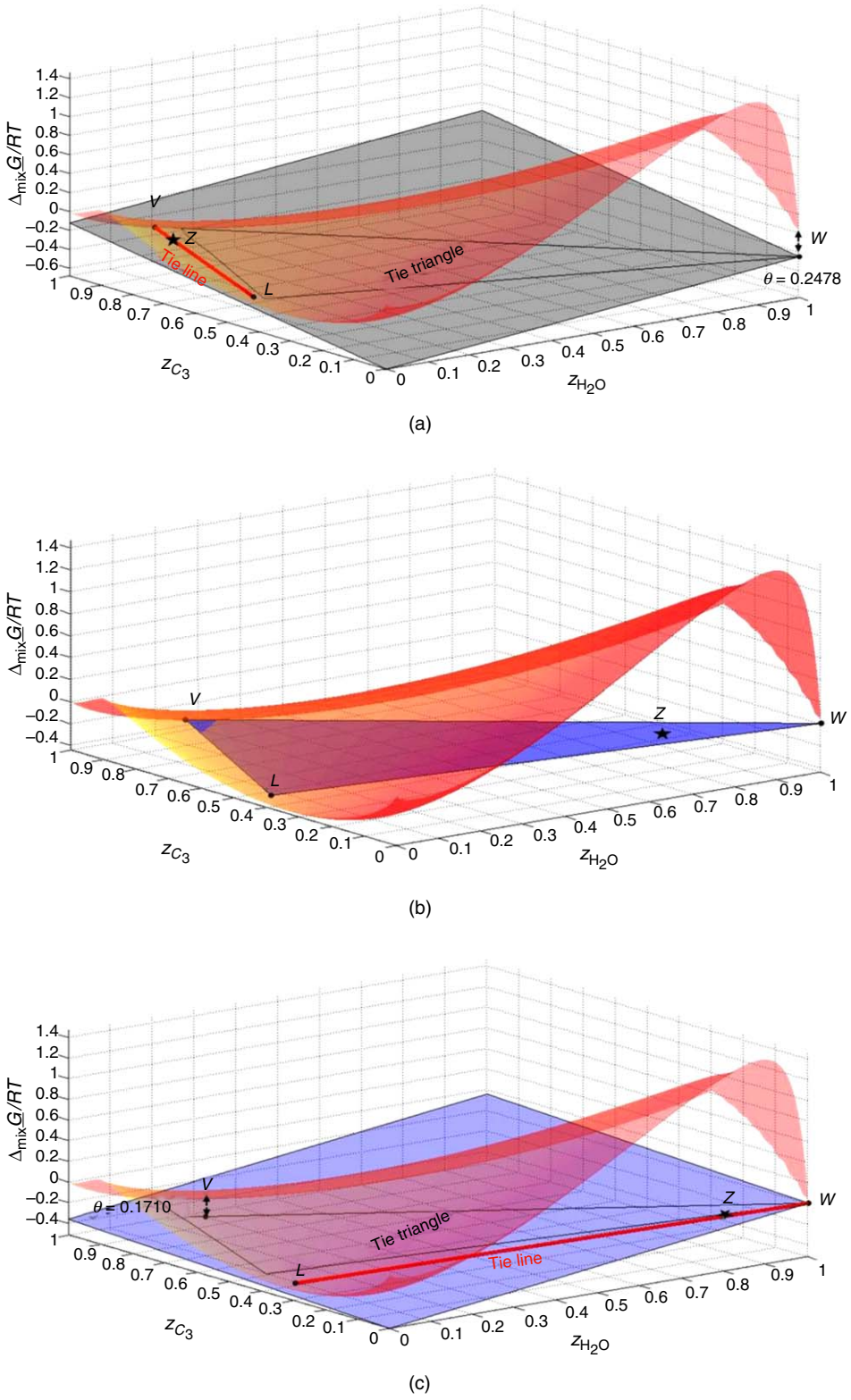

Fig. 2—Gibbs free energy surface at 430 K and 35 bar, and the tangent planes converged for three compositions on the mixing line given in Fig. 1. (a) $z_{H_2O} = 0.1$; (b) $z_{H_2O} = 0.75$; (c) $z_{H_2O} = 0.84$.

As an example for the new algorithm, **Fig. 4** shows the convergence behavior in terms of N_P and N_U, and the residual of Eq. 1, when it is initialized with $N_S = 6$ (i.e., three compositions near the compositional vertices and the other three at the centers of R_i for $i = 1$, 2, and 3 by use of $N_{Smax} = 6$ and $n = 1.0$). The new algorithm converges to the correct solution given in Table 2 in 21 iterations. Merging of sampling compositions (in set P and/or set U) occurs at the fourth, fifth, and seventh iterations, as indicated by decreasing N_S ($=N_U+N_P$) in Fig. 4a. Hence, the algorithm takes seven iteration steps to identify the correct number of stationary points in this case, when started with the six sampling compositions. A stable linear convergence rate is observed until the convergence is achieved, as with the normal successive substitution (Fig. 4b). The reference composition, $\underline{x}_r$, remains the same after the eighth iteration in this case. The total number of fugacity coefficient computations is 84, in which 25 computations were performed for initialization to determine a

reference composition; hence, on average, each iteration took approximately three computations of fugacity-coefficient vectors. Appendix D shows a series of ternary diagrams to explain the motion of sampling compositions for selected iterations.

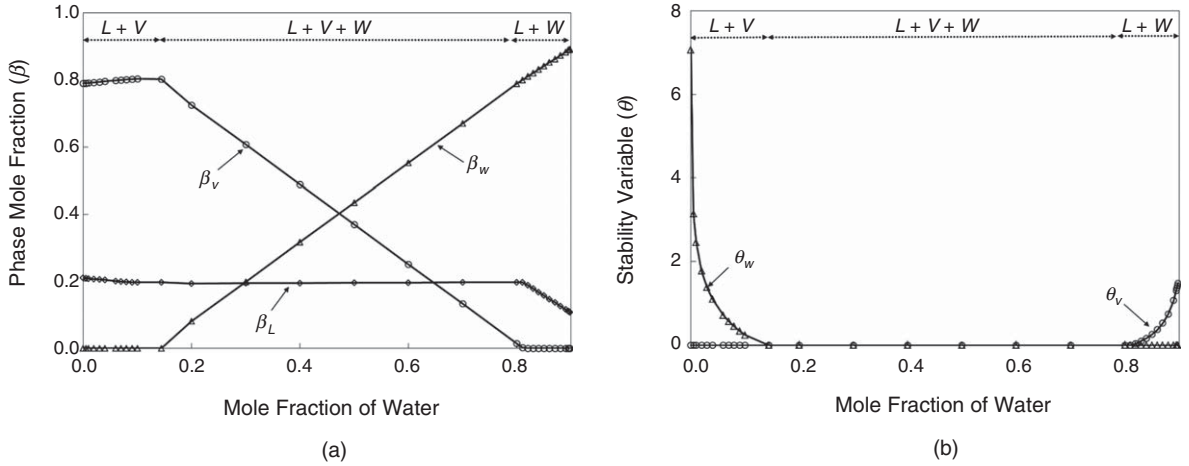

Fig. 3—Variation of parameters with the new algorithm applied along the mixing line given in Fig. 1, at 430 K and 35 bar. (a) Phase mole fraction. (b) Stability variable. $\theta_L = 0$ in Fig. 3b because the *L* phase is always present along the mixing line.

Component	*L*	*V*
H_2O	0.32452700	0.79574966
C_3	0.09549610	0.15586062
n-C_{16}	0.57997690	0.04838973
β	0.09708713	0.90291287
θ	0.00000000	0.00000000
$\underline{G_R}/RT$	–0.96787252	

Table 2—Solution for Case 1 with the new algorithm. Properties of the components are given in Table 1. The overall composition is 75% H_2O, 15% C_3, and 10% *n*-C_{16}. The specified temperature and pressure are 560 K and 65 bar, respectively. The algorithm of Gupta et al. (1991) fails for this case because of an open feasible domain in the RR problem based on their initialization scheme.

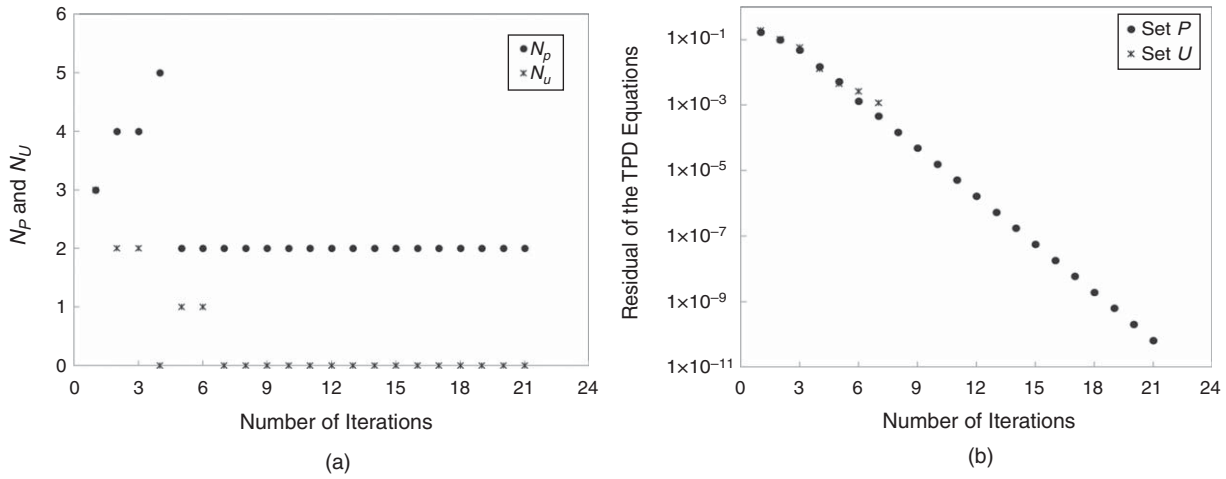

Fig. 4—Convergence behavior of the new algorithm for Case 1 with the overall composition of 75% H_2O, 15% C_3, and 10% *n*-C_{16} at 560 K and 65 bar. Properties of the components are given in Table 1. (a) N_P and N_U. (b) Residual of Eq. 1 for sets *P* and *U*.

It has been confirmed that the new algorithm still converges to the correct solution in 22 iteration steps when initialized with only three sampling compositions near the composition vertices for this relatively simple case. The total number of fugacity coefficient computations is 66, in which 13 computations were performed in initialization; hence, the average number of fugacity coefficient computations is three per iteration.

The conventional method of sequential phase-stability and -split calculation is also tested for this case. In the single-phase stability test, a trivial solution is detected in 53 iteration steps with a V-like composition for the first trial. Then, instability is detected in 14 iteration steps with an L-like composition for the second trial. Then, the subsequent two-phase-split calculation converges to the solution (Table 2) in 24 iterations. Phase instability cannot be detected with all nine guesses for this two-phase solution. The total number of iterations required in this two-phase stability test is 175. Hence, the total number of iterations required for the conventional sequential method is 266, compared with 21 for the new algorithm with $N_S = 6$. The total number of fugacity-coefficient computations is 301 with the conventional algorithm, in comparison with 84 with the new algorithm with $N_S = 6$. For this case, the new algorithm with $N_S = 6$ requires much fewer iterations and fugacity calculations than the conventional sequential algorithm.

Unlike in Gupta et al. (1991), the RR routine embedded in the new algorithm is guaranteed to converge to the correct solution as shown in Okuno et al. (2010a). It is important to confirm the existence of the unique solution for a given multiphase RR problem before the iteration (Okuno et al. 2010a).

Case 2. The simplicity of the formulation and algorithm developed in this research yields the robustness in multiphase flash by not having to obtain false solutions. The advantage over the conventional sequential methods is pronounced when the correct solution in a multiphase calculation does not include either the L_1 or V phase, which can frequently occur in many gas- and steam-injection processes with multiple partially miscible phases.

This case uses the binary system of C_1 and hydrogen sulfide (H_2S) at 190 K and 40.53 bar to show several issues of the sequential method and the robustness of the new algorithm. **Table 3** gives the components' properties. The Gibbs free energy surface in composition space exhibits three lobes corresponding to the L_1, L_2, and V phases in the order of increasing C_1 concentration (z_{C1}) **(Fig. 5).** The sequential method fails to find the correct solutions with L_2+V for z_{C1} from 0.968 to 0.982, as explained below.

Component	P_C (bar)	T_C (K)	ω
C_1	46.0016	190.6000	0.0080
H_2S	89.3686	373.2000	0.1000

Table 3—Properties of the components for Case 2. The binary interaction parameter between C_1 and H_2S is 0.0800.

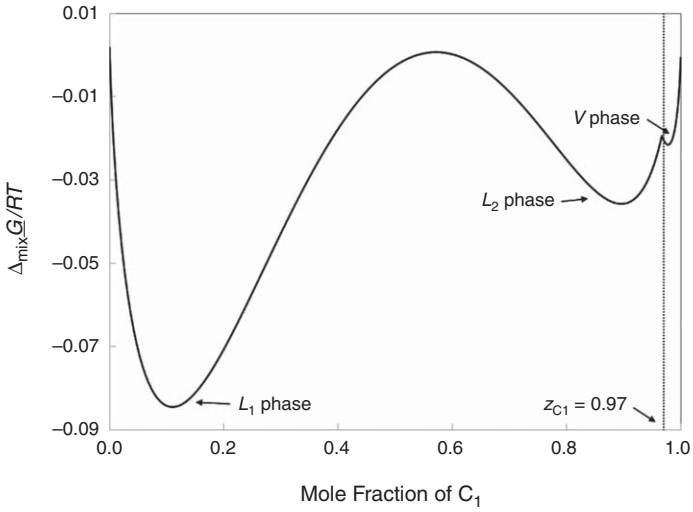

Fig. 5—Gibbs free energy surface in composition space for the binary system of C_1 and H_2S at 190 K and 40.53 bar. Properties of the components are given in Table 3. The three lobes indicated correspond to the L_1, L_2, and V phases in the order of increasing C_1 mole fraction in composition space.

For $0.968 \le z_{C1} < 0.980$, the sequential algorithm finds an L phase in the single-phase stability analysis, and the subsequent two-phase flash results in a local minimum with L_1+V. Then, the stability analysis for one of the two phases finds the L_2 phase. However, three-phase PT flash is not possible for a binary mixture, for which P and T are interdependent (i.e., the degree of freedom is one). Hence, the final result from the sequential algorithm is the L_1+V phases that have been obtained. **Table 4** shows the correct solution from the new algorithm and the incorrect solution from the sequential method at $z_{C1} = 0.970$ at 190 K and 40.53 bar.

	New Algorithm			Sequential Algorithm	
	L_1	V	L_2	L_1	V
C_1	0.18666898	0.98270136	0.93610375	0.12587785	0.97953529
H_2S	0.81333102	0.01729864	0.06389625	0.87412215	0.02046471
β	0.00000000	0.72742456	0.27257544	0.01116888	0.98883111
θ	0.13266274	0. 00000000	0. 00000000	–	–
$\underline{G}_R/RT$	–0.53949050			–0.53769775	

Table 4—Results for Case 2 with the new and conventional sequential algorithms. Properties of the components are given in Table 3. The overall composition is 97% C_1 and 3% H_2S for this table. The specified temperature and pressure are 190 K and 40.53 bar, respectively.

The new algorithm converges to the correct two-phase solution (L_2+V) directly without having to find any false solution. Here, the convergence of the new algorithm is explained for the case with initial $N_S = 8$ ($N_{S\max} = 16$ and $n = 1.0$). Two of them are distributed near the vertices of composition space, and three sampling compositions are evenly distributed for each side of the overall composition. **Fig. 6** shows the variation of N_P and N_U, and the residual of Eq. 1 with respect to the number of iterations for this case. The new algorithm successfully converges to the correct solution (Table 4) in 92 iterations. The converged Gibbs free energy ($\underline{G}_R$) from the new algorithm, −0.53949050, is confirmed to be lower than the value from the sequential method, −0.53769775.

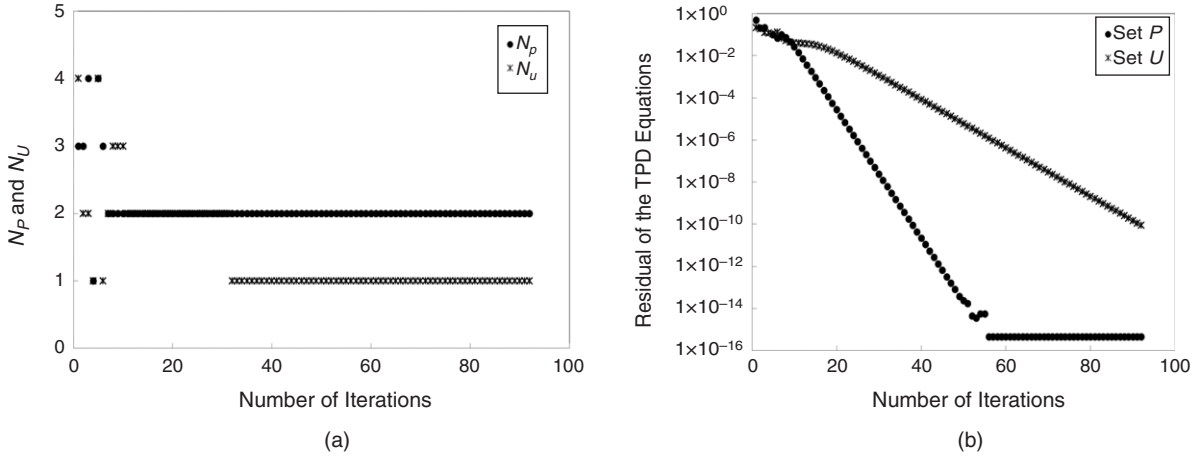

Fig. 6—Convergence behavior of the new algorithm for Case 2 at 190 K and 40.53 bar. Properties of the components are given in Table 3. (a) N_P and N_U. (b) Residual of Eq. 1 for sets P and U.

In the initialization, $N_P = 1$ occurs in the initialization, which increases N_S by one as the overall composition becomes part of the sampling compositions in such a case (Step 2 in the algorithm). Reselection of reference composition (Steps 7 and 8 of the new algorithm) occurs frequently from Iterations 1 through 6, in which Step 8 is only used at the fourth iteration and Step 7 at the other five iterations. Merging of sampling compositions occurs at the first, 10th, and 31st iterations, as shown by decreasing N_S ($=N_P+N_U$) in Fig. 6a. From the 31st iteration, N_S becomes the total number of stationary points, three, on the D_R function. At the convergence, two of the three stationary points correspond to the two equilibrium phases (i.e., set P), and the other is a nontangent stationary point (i.e., set U) with a positive D_R (Table 4). The residual of Eq. 1 shown in Fig. 6b indicates a linear convergence rate for a fixed reference composition, $\underline{x}_r$. The total number of fugacity-coefficient computations is 348, out of which 33 computations are performed in the initialization to determine a reference composition. The average number of fugacity-coefficient computations per iteration is approximately three. Appendix D demonstrates the motion of all sampling compositions for selected iteration steps, in which merging and convergence of sampling compositions are clearly shown.

To see the number of iterations required for robust convergence with respect to the initial N_S used, the initial N_S was controlled by changing $N_{S\max}$ by two with $n = 1.0$ with the procedure given in Appendix C. The initial N_S required for robust convergence is eight in this case. The numbers of iterations required for convergence are 92, 86, and 76 for the initial N_S of 8, 10, and 12. The number of stationary points detected upon convergence is three for $N_S \geq 8$. The numbers of fugacity-coefficient calculations are 348, 341, and 327 for the initial N_S of 8, 10, and 12.

When initialized with $N_S = 4$ (two near the edges of composition space and the other two at the centers of both sides of the overall composition), the algorithm does not converge to the global minimum of the Gibbs free energy. To explain this, **Fig. 7** shows the TPD in composition space at 190 K and 40.53 bar. The correct two-phase solution of L_2+V is represented by the black dots on the D_R function. The hollow square dot is a local minimum on D_R. Only two stationary points are located when the algorithm is initialized with only four sampling compositions. These two stationary points correspond to the L_1 and V lobes on the Gibbs free energy surface (Fig. 5), which do not yield the global minimum of the Gibbs free energy.

For $0.980 \leq z_{C1} \leq 0.982$, the sequential algorithm fails to find any phase instability in single-phase stability analysis. However, the new algorithm properly converges to the L_2 and V phases. **Table 5** shows the solution for z_{C1} of 0.980. The Gibbs free energy ($\underline{G}_R$) at the solution, –0.49203424, is confirmed to be lower than the single-phase Gibbs free energy, –0.49183831.

Even if the degree of freedom is more than one for the sequential method, it has been observed in various flow-simulation cases that the sequential method initiated with Wilson's K values tends to fail to find the correct solution that does not involve the L_1 or V phases. An example is the ternary mixture of 60% carbon dioxide (CO_2), 12% C_1, and 28% n-C_{20} at 250 K and 38 bar. Three phases of L_1, L_2, and V are present in composition space, and the overall composition in the L_1–L_2 region is in the vicinity of the tie triangle. The sequential method cannot find phase instability in the two-sided stability analysis with the V and L estimates from Wilson's correlation. Case 4 will provide another example of this kind.

Case 3. This case uses a mixture of North Ward Estes oil (Khan et al. 1992), H_2O, CO_2, n-C_4, and n-C_{10}. The North Ward Estes oil has been characterized with six components; therefore, there are 10 components altogether. Components' properties and the overall composition are given in **Table 6.** The critical endpoint of type $V = L_2$+L_1 is calculated by use of the PR EOS at 452.80 K and 86.04 bar for this mixture. Three equilibrium phases, $V + L_1$+L_2, coexist at 459 K and 87 bar (i.e., close to the critical endpoint).

The new algorithm is tested with different initial numbers of sampling compositions (N_S). For this purpose, N_S is controlled by changing $N_{S\max}$ from 20 to 95 by adding 15 with $n = 1.0$. The number of stationary points (minima) detected upon convergence is four for all initial N_S tested: three tangent stationary points (i.e., set P) and one nontangent stationary point (i.e., set U).

To explain this case specifically, the new algorithm is initialized with $N_S = 20$ ($N_C = 10$, $N_{S\max} = 20$, and $n = 1.0$). In addition to 10 sampling compositions placed near the 10 composition vertices, 10 sampling compositions are distributed at the central points of regions R_i for $i = 1, 2, \ldots, 10$ in composition space around the overall composition (Appendix C).

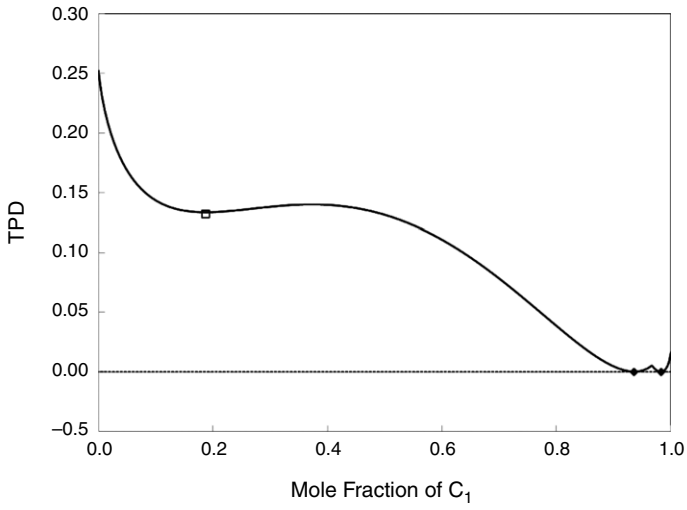

Fig. 7—TPD in composition space for the binary system of C_1 and H_2S. Properties of the components are given in Table 3. The temperature and pressure are 190 K and 40.53 bar, respectively.

Component	L_1	V	L_2
β	0.00000000	0.94202784	0.05797216
θ	0.13266274	0.00000000	0.00000000
$\underline{G_R}/RT$		–0.49203424	

Table 5—Solution for Case 2 with the new algorithm. Properties of the components are given in Table 3. The overall composition is 98% C_1 and 2% H_2S. The specified temperature and pressure are 190 K and 40.53 bar, respectively. The correct set of three phase compositions is identical to the one presented in Table 4. The conventional algorithm fails to find phase instability in single-phase stability analysis for this flash calculation.

Component	Overall Composition	MW (g/mol)	P_C (bar)	T_C (K)	ω
CO_2	0.1200	44.0100	73.7600	304.2000	0.2250
C_1	0.0489	16.0430	46.0000	190.6000	0.0080
n-C_4	0.4400	58.1240	38.0000	425.2000	0.1930
n-C_{10}	0.1000	142.2850	21.0800	617.6000	0.4900
C_{2-3}	0.1121	38.4000	45.0500	343.6400	0.1300
C_{4-6}	0.1000	72.8200	33.5100	466.4100	0.2440
C_{7-14}	0.0300	135.8200	24.2400	603.0700	0.6000
C_{15-24}	0.0100	257.7500	18.0300	733.7900	0.9030
C_{25+}	0.0090	479.9500	17.2600	923.2000	1.2290
H_2O	0.0300	18.0150	220.8900	647.3000	0.3440

Binary Interaction Parameters

	CO_2	C_1	n-C_4	n-C_{10}	C_{2-3}	C_{4-6}	C_{7-14}	C_{15-24}	C_{25+}	H_2O
CO_2	0.0000	0.1200	0.1200	0.1141	0.1200	0.1200	0.0900	0.0900	0.0900	0.6670
C_1	–	0.0000	0.0000	0.0422	0.0000	0.0000	0.0000	0.0000	0.0000	0.7320
n-C_4	–	–	0.0000	0.0078	0.0000	0.0000	0.0000	0.0000	0.0000	0.6840
n-C_{10}	–	–	–	0.0000	0.0000	0.0000	0.0000	0.0000	0.0000	0.3570
C_{2-3}	–	–	–	–	0.0000	0.0000	0.0000	0.0000	0.0000	0.6790
C_{4-6}	–	–	–	–	–	0.0000	0.0000	0.0000	0.0000	0.6050
C_{7-14}	–	–	–	–	–	–	0.0000	0.0000	0.0000	0.4910
C_{15-24}	–	–	–	–	–	–	–	0.0000	0.0000	0.3270
C_{25+}	–	–	–	–	–	–	–	–	0.0000	0.2420
H_2O	–	–	–	–	–	–	–	–	–	0.0000

Table 6—Properties of the components for Case 3. MW=molecular weight.

Fig. 8 shows the convergence behavior in terms of N_P, N_U, N_S, and the residual of Eq. 1 with the new algorithm. The new algorithm converges to the correct solution in 823 iterations, as shown in **Table 7,** in which the compositions of V and L_2 are close to each other. Upon convergence, three equilibrium compositions are in set P, and one nontangent stationary composition is in set U. The nontangent stationary point is converged near 100% water with $\theta = 0.79$. The Gibbs free energy ($\underline{G}_R$) converged with the new algorithm is –2.67985726.

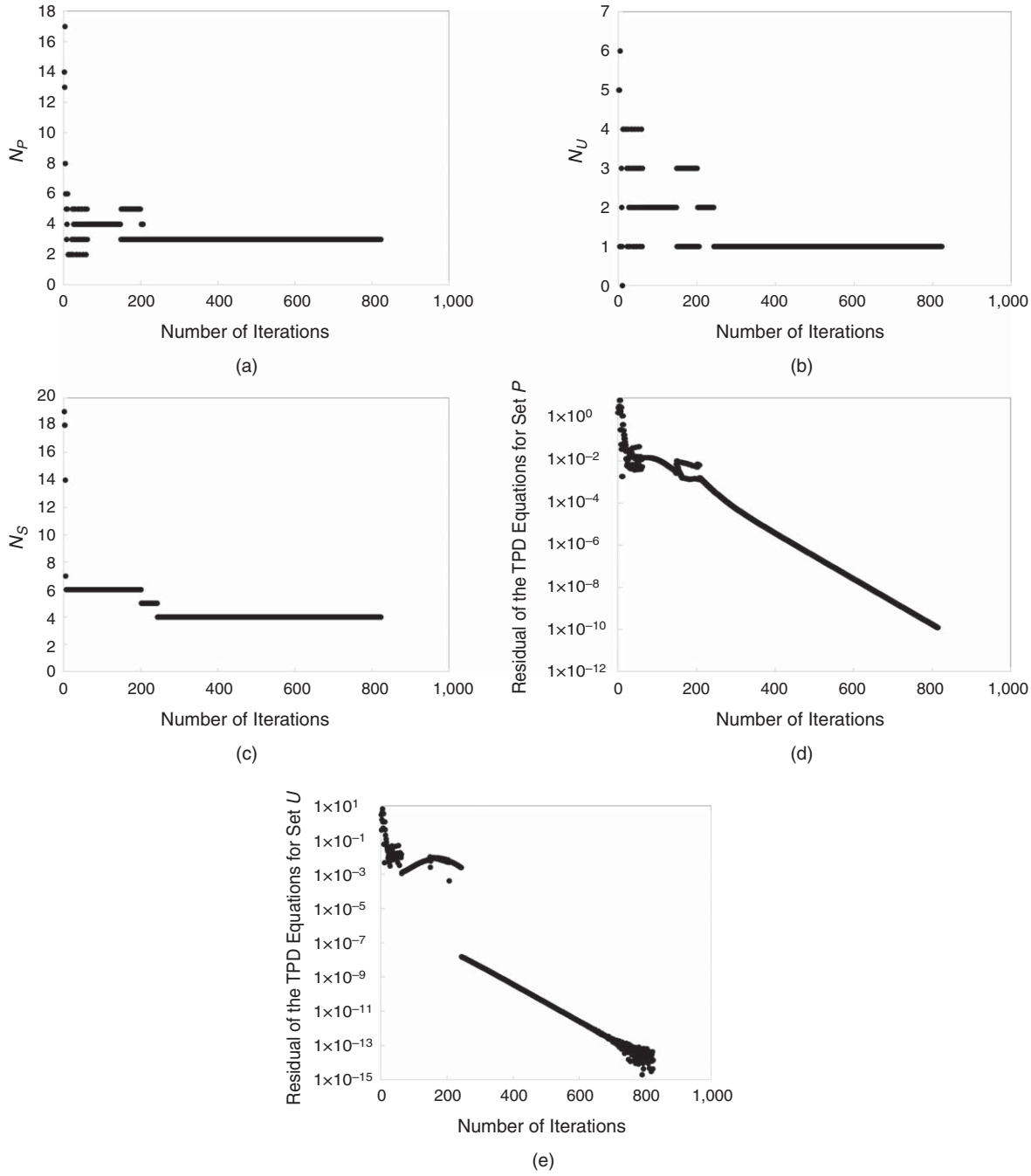

Fig. 8—Convergence behavior of the new algorithm for Case 3. Properties of the components are given in Table 6. The temperature and pressure are 459 K and 87 bar, respectively. (a) N_P; (b) N_U; (c) N_S; (d) residual of Eq. 1 for set P; and (e) residual of Eq. 1 for set U.

In the initialization, two sampling compositions are in set P, and the other 18 compositions are in set U. Merging of sampling compositions in set P and/or set U reduces N_S during the iteration (Fig. 8c). Reselection of the reference composition occurs frequently between Iterations 1 and 11, 21 and 62, and 148 and 206, resulting in the oscillation of N_P and N_U during these iterations (Figs. 8a and 8b). Accordingly, the residuals of Eq. 1 for sets P and U also exhibit oscillations, as can be seen in Figs. 8d and 8e. At the 206th iteration, the correct N_P of three is identified, from which the residual of Eq. 1 for set P starts decreasing steadily (Figs. 8a and 8d). At the 243rd iteration, N_U decreases from two to one, which makes the residual of Eq. 1 for set U decrease discontinuously, as presented in Figs. 8b and 8e. From the 243rd iteration on, a stable linear convergence rate is observed with the final number of stationary points ($N_P = 3$ and $N_U = 1$). Between the 700th and the 823rd iterations, the residual of Eq. 1 for set U exhibits oscillations around 10^{-14}, which is much lower than the convergence criteria (10^{-10} used in this paper). This is likely because, in this particular case, the residual for set U is sensitive to the TPD function, which is varying with varying compositions in set P before the final convergence (i.e., the TPD is defined with a reference composition in set P).

Component	L_2	L_1	V	Nontangent Stationary Point
CO_2	0.11738916	0.07803457	0.15787879	0.00010037
C_1	0.04753232	0.02844412	0.06839099	0.00002118
n-C_4	0.44144075	0.38822000	0.43634612	0.00000002
n-C_{10}	0.10303175	0.13284012	0.05967230	0.00000000
C_{2-3}	0.11120735	0.08458583	0.12808134	0.00000070
C_{4-6}	0.10094542	0.09554283	0.09080736	0.00000000
C_{7-14}	0.03083866	0.04300449	0.01794197	0.00000000
C_{15-24}	0.01029303	0.02618153	0.00310814	0.00000000
C_{25+}	0.00795880	0.09401603	0.00068515	0.00000000
H_2O	0.02936275	0.02913048	0.03708783	0.99987773
β	0.89781487	0.01911965	0.08306548	0.00000000
θ	0.00000000	0.00000000	0.00000000	0.79007647
$\underline{G_R}/RT$		–2.67985726		

Table 7—Results for Case 3 with the new algorithm.

The number of iterations required for convergence are 823 and 737 for the initial N_S of 20 ($N_{S\max} = 20$ with $n = 1.0$) and 40 ($N_{S\max} = 96$ with $n = 1.0$), respectively. For N_S of 20, the total number of fugacity-coefficient computations is 3,861, out of which 81 computations are for the initialization. Therefore, the number of fugacity calculations per iteration is approximately five for this case.

The conventional sequential phase-stability and -split calculation is also tested for this case. **Fig. 9** shows the number of iterations required for each step of the conventional sequential method. The initialization procedure for the conventional method was explained earlier in this section. Single-phase stability analysis detects an instability with a V-like phase composition at the 96th iteration. Then, the subsequent two-phase-split calculation converges to a false two-phase solution in 456 iterations. After that, two-phase stability analysis detects an instability of the two-phase solution by use of the second initial guess. The first guess takes 128 iterations, but they are unable to identify any phase instability. The second guess then takes 166 iterations until phase instability is detected. A three-phase split calculation is performed with the initial K value estimates obtained from the two-phase-stability test, and converges to a solution in 708 iterations. Phase instability cannot be detected for this three-phase solution by use of all 23 sets of initial guesses. The number of iterations taken by this three-phase stability analysis is 9,782. That is, the conventional sequential method requires 11,336 iterations for its final solution of three phases. The total number of fugacity-coefficient calculations is 13,234 with the sequential method. Computations in the three-phase stability are counted for a fair comparison with the new algorithm because the new algorithm has found a nontangent stationary point, as shown in Table 7. However, the new algorithm is shown to require fewer iterations and fugacity computations even without considering the three-phase stability for the sequential method. These results show that the convergence of the new algorithm is more rapid than that of the sequential algorithm in terms of iteration and fugacity calculation for this case.

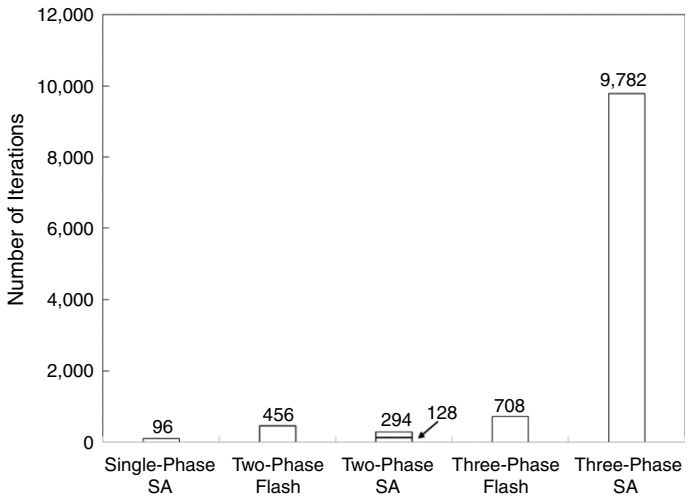

Fig. 9—Number of iterations required for each step in the conventional sequential method of PT flash for Case 3. The total number of iterations required for convergence by use of the conventional sequential algorithm is 11,336, if the number of iterations for the initial guesses that cannot identify phase instability for two and three phases is counted. SA = stability test.

Case 4. Case 4 uses a four-component EOS fluid model based on the Bob Slaughter Block (BSB) oil that was originally characterized by Khan et al. (1992) with seven components. This quaternary model for the BSB oil (BSB-Q) was used previously in Okuno et al. (2011). Parameters for the BSB-Q oil are given in **Table 8.** The new and conventional algorithms are compared for flash calculation of the BSB-Q oil at 313.706 K and 82.737 bar.

Component	Overall Composition	T_C (K)	P_C (bar)	ω
CO_2	0.7218	304.200	73.765	0.225
C_1	0.0214	160.000	46.002	0.008
PC1	0.1870	529.028	27.318	0.481
PC2	0.0698	795.328	17.309	1.042
Binary Interaction Parameters				
	CO_2	C_1	PC1	PC2
CO_2	0.0000	0.0550	0.0810	0.1050
C_1	–	0.0000	0.0000	0.0000
PC1	–	–	0.0000	0.0000
PC2	–	–	–	0.0000

Table 8—Properties of the components for Case 4. PC = pseudocomponent.

The new algorithm converges to two tangent stationary points (L_1 and L_2) in set P and one nontangent stationary point (V) in set U, when 12 or more sampling compositions are initially distributed by use of the method given in Appendix C. **Table 9** summarizes the converged solution.

Component	V	L_1	L_2
CO_2	0.92939195	0.62612349	0.86182262
C_1	0.05933155	0.01782033	0.02660759
PC1	0.01127539	0.24083442	0.10820073
PC2	0.00000111	0.11522177	0.00336906
β	0.00000000	0.59418965	0.40581035
θ	0.00154683	0. 00000000	0. 00000000

Table 9—Results for Case 4 with the new algorithm.

For the initial N_S of 12, the convergence is achieved in 161 iterations. The converged $\underline{G}_R$ value is -3.45251125. The total number of fugacity-coefficient vector computations is 720, of which 49 computations are for the initialization. The number of fugacity-coefficient vector computations is approximately four per iteration. **Fig. 10** shows the convergence behavior of the new algorithm. It requires 42 iterations to identify the correct number of stationary points; i.e., $N_P = 2$ and $N_U = 1$ (Figs. 10a and 10b). Merging of sampling compositions occurs at iteration steps 8, 11, 16, 19, 20, 21, 23, 37, and 42, resulting in reduction of N_S as shown in Fig. 10c. Reselection of the reference composition, $\underline{x}_r$, by use of Steps 7 and 8 of the new algorithm occurs frequently until the 26th iteration. At the 42nd iteration, N_U becomes the final number of nontangent stationary points through merging, resulting in a significant decrease in the residual for set U (Fig. 10e).

The conventional sequential method is shown to converge to an incorrect solution for this case. **Fig. 11** shows the number of iterations required for each step of the sequential phase-stability and -split calculations. The single-phase stability finds an instability with a V-like initial composition (i.e., the first guess) in 18 iterations. Then, the subsequent two-phase flash converges in 47 iterations. After that, two-phase stability analysis with six different estimates finds no instability after the total of 688 iterations. With the seventh initial guess (i.e., the midpoint), an instability is detected in 128 iterations. Three-phase flash is performed with the initial K values obtained from two-phase stability analysis and converges in 141 iterations. This three-phase flash results in negative phase amounts; i.e., negative flash. Hence, another two-phase flash is performed, and it converges in 49 iterations. Then, phase-stability analysis for the new two-phase solution with 11 different initial guesses finds no instability, taking 855 iterations. Finally, two phases are assumed to be stable after the total of 1,926 iterations. The number of fugacity-coefficient vector calculations is 2,323. However, the converged $\underline{G}_R$ value is -3.45110691, which is higher than the $\underline{G}_R$ obtained from the new algorithm (-3.45251125). This indicates that the two-phase solution obtained from the conventional sequential method is a local minimum of Gibbs free energy. The new algorithm converged to a lower Gibbs free energy with much fewer iterations and fugacity computations.

The new algorithm based on successive substitution can be used to initialize a second-order convergent method with set P, as mentioned previously. Here, the current case is used to show the convergence behavior of the new algorithm and an in-house second-order algorithm (Okuno et al. 2010b) with different switching criteria. The final convergence criterion used for the second-order algorithm is 10^{-10}, as in all case studies in this paper. The switching criterion used with Eq. 1 for sets P and U ranges from 10^{-2} to 10^{-6}. **Table 10** summarizes the number of iterations for the new algorithm before switching and the second-order algorithm after switching for each of the switching criteria used. After switching to the second-order algorithm, the correct convergence is achieved rapidly in three or fewer iterations for all the cases tested. As an example, the convergence behavior before and after switching is shown in Fig. 10d with the switching criterion of 10^{-2}. The new algorithm is used until the 38th iteration, and is switched to the second-order algorithm when the residual of Eq. 1 is below 10^{-2} for both sets P and U. Then, the rapid convergence is achieved in three iterations, as shown by the star markers in Fig. 10d. The total number of iterations required for convergence is 41. Use of the second-order algorithm after switching at 10^{-2} results in four times more rapid convergence in terms of number of iterations compared with the use of the new algorithm alone.

Another test is conducted by use of Wilson's correlation to initialize the new algorithm with only two sampling compositions: one V-like and one L-like. The new algorithm converges in 190 iterations to the same solution presented in Table 9; i.e., two tangent stationary points (L_1 and L_2) in set P and one nontangent stationary point (V-like) in set U. The total number of fugacity-coefficient vector

computations is 582, of which nine computations are for the initialization. Hence, the number of fugacity-coefficient vector computations is approximately three per iteration.

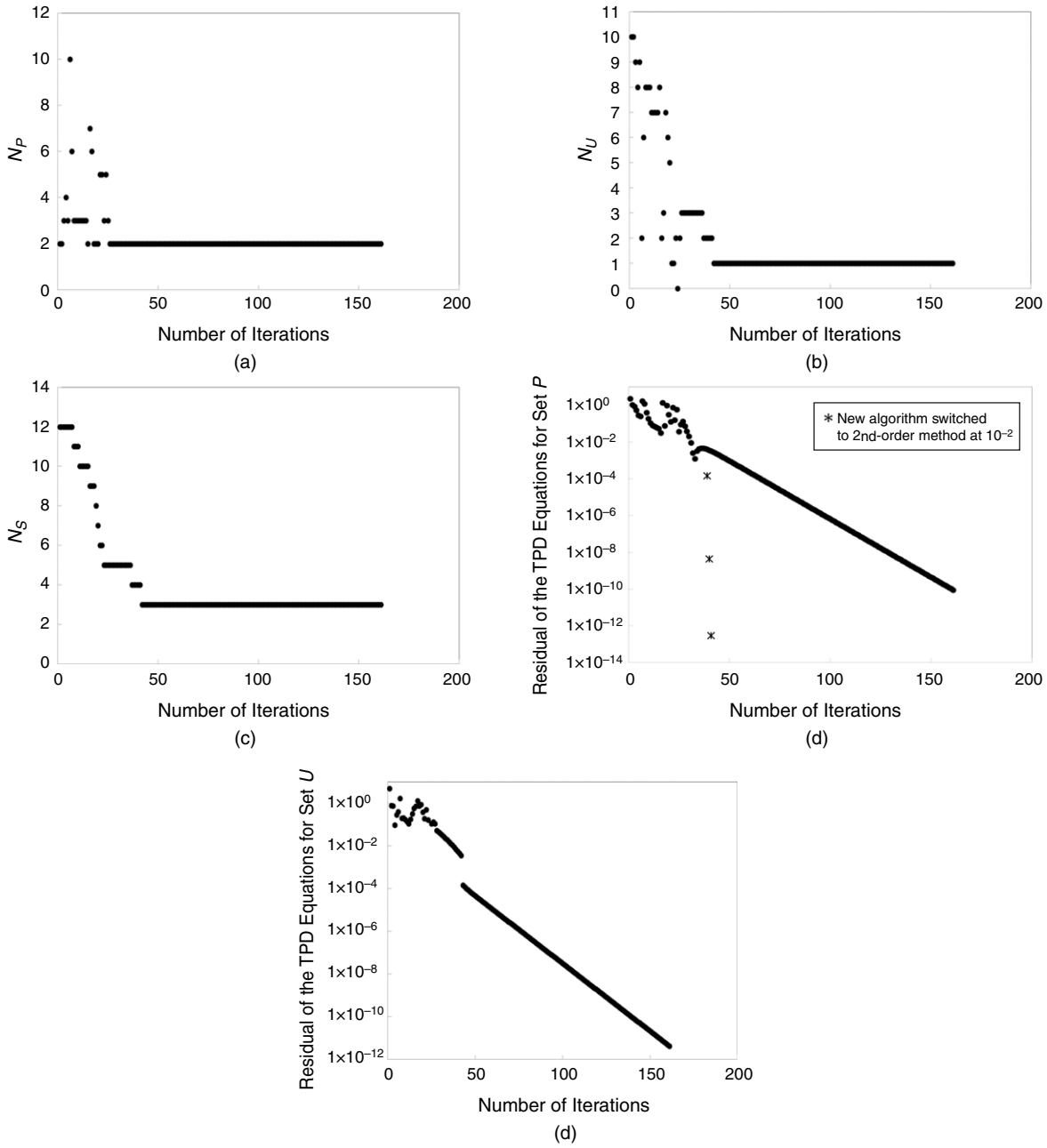

Fig. 10—Convergence behavior of the new algorithm for Case 4. Properties of the components are given in Table 8. The temperature and pressure are 313.706 K and 82.737 bar, respectively. (a) N_P; (b) N_U; (c) N_S; (d) residual of Eq. 1 for set *P*; and (e) residual of Eq. 1 for set *U*. Fig. 10d also shows the convergence behavior of a second-order convergent method that has been initialized by the new algorithm with the switching criterion of 10^{-2} for Eq. 1 for sets *P* and *U*.

Fig. 12 shows the convergence behavior of the new algorithm. The correct number of stationary points [i.e., $N_P = 2$ and $N_U = 1$ (Figs. 12a and 12b)] is identified at the 55th iteration. In the initialization, $N_P = 1$ occurs, which increases N_S by one when the overall composition becomes an additional sampling composition (Step 2). Merging of sampling compositions does not occur for this case. Hence, N_S remains three until the final convergence is achieved. Reselection of reference composition, $\underline{x}_r$, by use of Steps 7 and 8 of the new algorithm occurs at iteration steps 1, 2, 20, and 55. In Fig. 12c, a significant increase in the residual of the TPD equations occurs for set *P* at the 20th iteration when N_P is increased from two to three. N_U is zero between iteration steps 20 and 54, for which the residual of the TPD equations for set *U* does not exist in Fig. 12d. From the 55th iteration until the convergence, N_P and N_U are the final numbers of tangent stationary points and nontangent stationary points: two and one, respectively.

It was observed that the current algorithm could exhibit nonconvergence when the binary interaction parameters of PC2 with C_1 and PC1 were set to –0.5. Hence, the current algorithm is considered to possess the inherent limitation of successive substitution (Heidemann and Michelsen 1995), as mentioned at the beginning of this section.

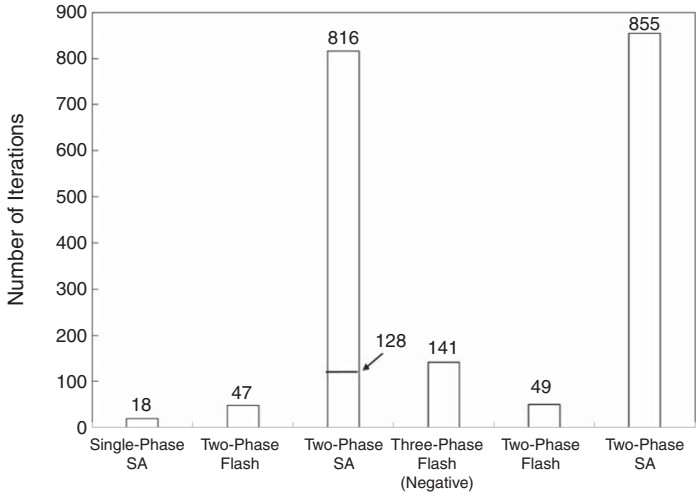

Fig. 11—Number of iterations required for each step in the conventional sequential method of PT flash for Case 4. The total number of iterations required for convergence by use of the conventional sequential algorithm is 1,926, if the number of iterations for the initial guesses that cannot identify phase instability for two and three phases is counted. SA = stability test.

Switching Criterion	10^{-2}	10^{-3}	10^{-4}	10^{-5}	10^{-6}
Number of iterations required for the new algorithm	38	50	66	82	98
Number of iterations required for the second-order method	3	2	2	2	1
Total number of iterations required for final convergence	41	52	68	84	99

Table 10—Number of iterations when the new algorithm is used to initialize a second-order convergent method for Case 4.

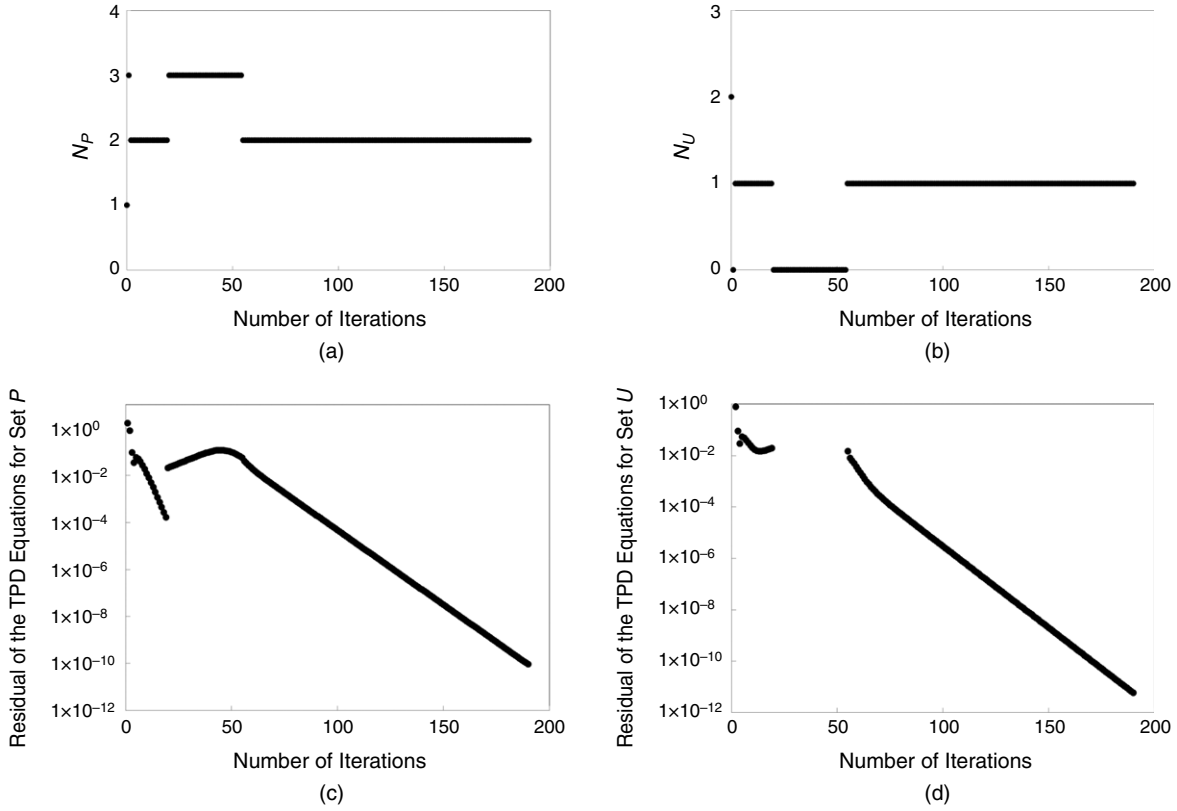

Fig. 12—Convergence behavior of the new algorithm for Case 4 with the use of Wilson's correlation in the initialization (i.e., one *V*-like and one *L*-like composition). Properties of the components are given in Table 8. The temperature and pressure are 313.706 K and 82.737 bar, respectively. (a) N_P; (b) N_U; (c) N_S; (d) residual of Eq. 1 for set *P*; and (e) residual of Eq. 1 for set *U*.

Conclusions

This paper presented a new algorithm for PT flash for an arbitrary number of phases. The unified formulation developed for simultaneous phase-stability and -split calculation is based on the classical criterion of phase equilibrium, as explained in Baker et al. (1982). The

correct set of equations is solved with successive substitution for stationary points of the TPD defined at a reference phase composition. Although the main focus of this paper was on robust solution of multiphase flash, the new algorithm can be used also to initialize a second-order convergent method in the vicinity of a solution. Conclusions are as follows:

1. The number of equilibrium phases is part of the solution in the new algorithm, in contrast to the sequential stability/flash approach. It is not necessary to find false solutions and correct them for robust multiphase flash with the new algorithm. The advantage of the new algorithm in terms of robustness is more pronounced for more-complex phase behavior, in which multiple local minima of the Gibbs free energy are present.
2. The new algorithm can be initialized even when no reliable information is available regarding the equilibrium phases of the fluid of interest. In the method used for initializing the algorithm, N_C sampling compositions are distributed near compositional vertices, and the others are systematically distributed around the overall composition specified. No K value correlation is necessary to initialize the new algorithm. This also yields the flexibility that the new algorithm offers in terms of robustness and efficiency. For example, one can initialize the algorithm with more sampling compositions for enhanced robustness by capturing more information regarding the Gibbs free energy during the iteration. If reasonable estimates are available for equilibrium phases (e.g., correlations, the solution from the previous timestep in flow simulation, and tie-simplex tabulation), one can use them to reduce the number of equations to be solved.
3. The new algorithm does not use the stability equations of Gupta et al. (1991) because they are not necessary with the formulation presented in this research. Consequently, there is no need to solve the augmented Jacobian matrix that must be solved at each iteration in the algorithm of Gupta et al. (1991). Also, the new algorithm does not exhibit the convergence problems that are associated with the stability equations of Gupta et al. (1991).
4. Case studies showed that the new algorithm finds more-stable solutions (lower Gibbs free energy) for the complex cases tested, for which the conventional method only finds local minima. It was shown that the new algorithm can find nontangent stationary points of the TPD function, if present, in addition to equilibrium phases.
5. The iteration scheme of the new algorithm is the traditional successive substitution, of which convergence behavior has been studied in the literature (Michelsen 1982a; Mehra et al. 1983; Ammar and Renon 1987; Kaul 1992). The new algorithm can be used to initialize a second-order convergent method, as demonstrated in Case 4. It is expected to be more difficult for the algorithm to converge for mixtures that exhibit a large negative deviation from an ideal solution, according to the analysis of Heidemann and Michelsen (1995).

Nomenclature

D = tangent plane distance defined in Eqs. A-6 and A-10
D_{Rj} = dimensionless TPD defined in Eqs. A-13 and A-14
f_{ij} = residual of the tangent-plane equations defined in Eq. 1
g_j = residuals of the material-balance equations defined in Eq. 3
$\underline{G}_R$ = dimensionless molar Gibbs free energy defined in Eq. A-1
K_{ij} = K value for component i in phase j
$\underline{K}_j$ = vector consisting of N_C K values for phase j
L_1 = oil-rich liquid phase
L_2 = solvent-rich liquid phase
n = exponent used in distribution in Appendix C
N_C = number of components
N_P = number of sampling compositions in set P
N_S = number of sampling compositions
N_{Si} = number of sampling compositions distributed in R_i defined in Appendix C
$N_{S\max}$ = maximum number of initial sampling compositions used in distribution in Appendix C
N_U = number of sampling compositions in set U
P = pressure
P_C = critical pressure
r_{1i} = number of segments used in Step 4 in Appendix C
r_{2i} = number of segments used in Step 6 in Appendix C
R = universal gas constant
R_i = region defined in Step 2 in Appendix C
t_i = parameter defined in Eq. 3
T = temperature
T_C = critical temperature
$T(\underline{x})$ = tangent plane defined in Eq. A-5
V = gaseous phase
W = aqueous phase
x_{ij} = mole fraction of component i in phase j
$\vec{x}_j$ = vector consisting of N_C concentrations for phase j
X_i = parameter defined in Eq. A-12
z_i = overall mole fraction of component i
β_j = mole fraction of phase j
ε = convergence or merging criterion (e.g., 10^{-10} for convergence and 10^{-3} for merging)
θ_j = parameter for phase j as calculated by Eq. 4
φ_{ij} = fugacity coefficient of component i in phase j
ω = acentric factor

Subscripts

C = critical property
i = component index
j = phase index
mix = mixing

r = reference composition
R = dimensionless property
Ref = reference phase

Superscript
k = iteration step number

Acknowledgments

This research was supported by grants from Japan Petroleum Exploration Company Limited and Japan Canada Oil Sands Limited through the Center for Petroleum and Geosystems Engineering at the University of Texas at Austin. Di Zhu also received financial support from the China Scholarship Council.

References

Abdel-Ghani, R. M. 1995. *EOS Mixing Rules for Multi-Phase Behaviour*. Master's thesis, the University of Calgary.

Alsaifi, N. M. and Englezos, P. 2011. Prediction of Multiphase Equilibrium Using the PC-SAFT Equation of State and Simultaneous Testing of Phase Stability. *Fluid Phase Equilibr.* **302** (1–2): 169–178. https://doi.org/10.1016/j.fluid.2010.09.002.

Ammar, M. N. and Renon, H. 1987. The Isothermal Flash Problem: New Methods for Phase Split Calculations. *AIChE J.* **33** (6): 926–939. https://doi.org/10.1002/aic.690330606.

Baker, L. E., Pierce, A. C., and Luks, K. D. 1982. Gibbs Energy Analysis of Phase Equilibria. *SPE J.* **22** (5): 731–742. SPE-9806-PA. https://doi.org/10.2118/9806-PA.

Broyden, C. G. 1970a. The Convergence of a Class of Double-Rank Minimization Algorithms: 1. General Considerations. *IMA J. Appl. Math.* **6** (1): 76–90. https://doi.org/10.1093/imamat/6.1.76.

Broyden, C. G. 1970b. The Convergence of a Class of Double-Rank Minimization Algorithms: 2. The New Algorithm. *IMA J. Appl. Math.* **6** (3): 222–231. https://doi.org/10.1093/imamat/6.3.222.

Burgos-Solórzano, G. I., Brennecke, J. F., and Stadtherr, M. A. 2004. Validated Computing Approach for High-Pressure Chemical and Multiphase Equilibrium. *Fluid Phase Equilibr.* **219** (2): 245–255. https://doi.org/10.1016/j.fluid.2003.12.013.

Chaikunchuensakun, S., Stiel, L. I., and Baker, E. L. 2002. A Combined Algorithm for Stability and Phase Equilibrium by Gibbs Free Energy Minimization. *Ind. Eng. Chem. Res.* **41** (16): 4132–4140. https://doi.org/10.1021/ie011030t.

Firoozabadi, A. 1999. *Thermodynamics of Hydrocarbon Reservoirs*, first edition. New York City: McGraw-Hill Education.

Fletcher, R. 1970. A New Approach to Variable Metric Algorithms. *Comput. J.* **13** (3): 317–322. https://doi.org/10.1093/comjnl/13.3.317.

Gao, J., Okuno, R., and Li, H. A. 2016. An Experimental Study of Multiphase Behavior for *n*-Butane/Bitumen/Water Mixtures. *SPE J.* **22** (3): 783–798. SPE-180736-PA. https://doi.org/10.2118/180736-PA.

Gautam, R. and Seider, W. D. 1979. Computation of Phase and Chemical Equilibrium: Part I. Local and Constrained Minima in Gibbs Free Energy. *AIChE J.* **25** (6): 991–999. https://doi.org/10.1002/aic.690250610.

Goldfarb, D. 1970. A Family of Variable-Metric Methods Derived by Variational Means. *Math. Comput.* **24** (109): 23–26. https://doi.org/10.2307/2004873.

Goldfarb, D. 1976. Factorized Variable Metric Methods for Unconstrained Optimization. *Math. Comput.* **30** (136): 796–811. https://doi.org/10.2307/2005399.

Gill, P. E. and Murray, W. 1974. Newton-Type Methods for Unconstrained and Linearly Constrained Optimization. *Math. Program.* **7** (3): 311–350. https://doi.org/10.1007/BF01585529.

Gupta, A. K. 1990. *Steady State Simulation of Chemical Process*. PhD dissertation, University of Calgary.

Gupta, A. K., Bishnoi, P. R., and Kalogerakis, N. 1991. A Method for the Simultaneous Phase Equilibria and Stability Calculations for Multiphase Reacting and Non-Reacting Systems. *Fluid Phase Equilibr.* **63** (1–2): 65–89. https://doi.org/10.1016/0378-3812(91)80021-M.

Han, G. and Rangaiah, G. P. 1998. A Method for Multiphase Equilibrium Calculations. *Comput. Chem. Eng.* **22** (7–8): 897–911. https://doi.org/10.1016/S0098-1354(97)00223-8.

Heidemann, R. A. and Michelsen, M. L. 1995. Instability of Successive Substitution. *Ind. Eng. Chem. Res.* **34** (3): 958–966. https://doi.org/10.1021/ie00042a032.

Hua, J. Z., Brennecke, J. F., and Stadtherr, M. A. 1996. Reliable Prediction of Phase Stability Using an Interval Newton Method. *Fluid Phase Equilibr.* **116** (1–2): 52–59. https://doi.org/10.1016/0378-3812(95)02871-4.

Hua, J. Z., Brennecke, J. F., and Stadtherr, M. A. 1998a. Enhanced Interval Analysis for Phase Atability: Cubic Equation of State Models. *Ind. Eng. Chem. Res.* **37** (4): 1519–1527. https://doi.org/10.1021/ie970535+.

Hua, J. Z., Brennecke, J. F., and Stadtherr, M. A. 1998b. Reliable Computation of Phase Stability Using Interval Analysis: Cubic Equation of State Models. *Comput. Chem. Eng.* **22** (9): 1207–1214. https://doi.org/10.1016/S0098-1354(98)00024-6.

Iranshahr, A., Voskov, D., and Tchelepi, H. A. 2010. Generalized Negative-Flash Method for Multiphase Multicomponent Systems. *Fluid Phase Equilibr.* **299** (2): 272–284. https://doi.org/10.1016/j.fluid.2010.09.022.

Kaul, P. K. 1992. *A New and Efficient Approach for Two Phase Equilibrium Prediction Using Cubic Equations of State*. Master's thesis, Mississippi State University, Starkville, Mississippi.

Khan, S. A., Pope, G. A., and Sepehrnoori, K. 1992. Fluid Characterization of Three-Phase CO_2/Oil Mixtures. Presented at the SPE/DOE Enhanced Oil Recovery Symposium, Tulsa, 22–24 April. SPE-24130-MS. https://doi.org/10.2118/24130-MS.

Li, Z. and Firoozabadi, A. 2012. General Strategy for Stability Testing and Phase-Split Calculation in Two and Three Phases. *SPE J.* **17** (4): 1096–1107. SPE-129844-PA. https://doi.org/10.2118/129844-PA.

Litvak, M. L. 1994. New Procedure for Phase-Equilibrium Computations in Compositional Reservoir Simulators. *SPE Advanced Technology Series* **2** (2): 113–121. SPE-25252-PA. https://doi.org/10.2118/25252-PA.

Lucia, A. and Macchietto, S. 1983. New Approach to Approximation of Quantities Involving Physical Properties Derivatives in Equation-Oriented Process Design. *AIChE J.* **29** (5): 705–712. https://doi.org/10.1002/aic.690290502.

Lucia, A., Miller, D. C., and Kumar, A. 1985. Thermodynamically Consistent Quasi-Newton Formulae. *AIChE J.* **31** (8): 1381–1388. https://doi.org/10.1002/aic.690310817.

Lucia, A. and Liu, D. 1998. An Acceleration Method for Dogleg Methods in Simple Singular Regions. *Ind. Eng. Chem. Res.* **37** (4): 1358–1363. https://doi.org/10.1021/ie970681f.

Lucia, A., Padmanabhan, L., and Venkataraman, S. 2000. Multiphase Equilibrium Flash Calculations. *Comput. Chem. Eng.* **24** (12): 2557–2569. https://doi.org/10.1016/S0098-1354(00)00563-9.

Lucia, A. and Feng, Y. 2003. Multivariable Terrain Methods. *AIChE J* **49** (10): 2553–2563. https://doi.org/10.1002/aic.690491010.

Lucia, A., Bonk, B. M., Waterman, R. R. et al. 2012. A Multi-Scale Framework for Multi-Phase Equilibrium Flash. *Comput. Chem. Eng.* **36:** 79–98. https://doi.org/10.1016/j.compchemeng.2011.07.011.

Mehra, R. K., Heidemann, R. A., and Aziz, K. 1982. Computation of Multiphase Equilibrium for Compositional Simulation. *SPE J.* **22** (1): 61–68. SPE-9232-PA. https://doi.org/10.2118/9232-PA.

Mehra, R. K., Heidemann, R. A., and Aziz, K. 1983. An Accelerated Successive Substitution Algorithm. *Can. J. Chem. Eng.* **61** (4): 590–596. https://doi.org/10.1002/cjce.5450610414.

Michelsen, M. L. 1982a. The Isothermal Flash Problem. Part I. Stability. *Fluid Phase Equilibr.* **9** (1): 1–19. https://doi.org/10.1016/0378-3812(82)85001-2.

Michelsen, M. L. 1982b. The Isothermal Flash Problem. Part II. Phase-Split Calculation. *Fluid Phase Equilibr.* **9** (1): 21–40. https://doi.org/10.1016/0378-3812(82)85002-4.

Michelsen, M. L. 1994. Calculation of Multiphase Equilibrium. *Comput. Chem. Eng.* **18** (7): 545–550. https://doi.org/10.1016/0098-1354(93)E0017-4.

Michelsen, M. L. and Mollerup, J. M. 2004. *Thermodynamic Models: Fundamentals and Computational Aspects*. Holte, Denmark: Tie-Line Publications.

Nghiem, L. X. and Li, Y. K. 1984. Computation of Multiphase Equilibrium Phenomena with an Equation of State. *Fluid Phase Equilibr.* **17** (1): 77–95. https://doi.org/10.1016/0378-3812(84)80013-8.

Nghiem, L. X., Aziz, K., and Li, Y. K. 1983. A Robust Iterative Method for Flash Calculations Using the Soave-Redlich-Kwong or the Peng-Robinson Equation of State. *SPE J.* **23** (3): 521–530. SPE-8285-PA. https://doi.org/10.2118/8285-PA.

Ohanomah, M. O. and Thompson, D. W. 1984. Computation of Multicomponent Phase Equilibria-Part I. Vapor-Liquid Equilibria. *Comput. Chem. Eng.* **8** (3–4): 147–156. https://doi.org/10.1016/0098-1354(84)87001-5.

Okuno, R. 2009. *Modeling of Multiphase Behavior for Gas Flooding Simulation*. PhD dissertation, University of Texas at Austin, Austin, Texas.

Okuno, R., Johns, R. T., and Sepehrnoori, K. 2010a. A New Algorithm for Rachford-Rice for Multiphase Compositional Simulation. *SPE J.* **15** (2): 313–325. SPE-117752-PA. https://doi.org/10.2118/117752-PA.

Okuno, R., Johns, R. T., and Sepehrnoori, K. 2010b. Three-Phase Flash in Compositional Simulation Using a Reduced Method. *SPE J.* **15** (3): 689–703. SPE-125226-PA. https://doi.org/10.2118/125226-PA.

Okuno, R., Johns, R. T., and Sepehrnoori, K. 2011. Mechanisms for High Displacement Efficiency of Low-Temperature CO_2 Floods. *SPE J.* **16** (4): 751–767. SPE-129846-PA. https://doi.org/10.2118/129846-PA.

Pan, H. and Firoozabadi, A. 2003. Fast and Robust Algorithm for Compositional Modeling: Part II—Two-Phase Flash Computations. *SPE J.* **8** (4): 380–391. SPE-87335-PA. https://doi.org/10.2118/87335-PA.

Peng, D.-Y., and Robinson, D. B. 1976. A New Two-Constant Equation of State. *Ind. Eng. Chem. Fundamen.* **15** (1): 59–64. https://doi.org/10.1021/i160057a011.

Peng, D.-Y., and Robinson, D. B. 1978. The Characterization of the Heptanes and Heavier Fractions for the GPA Peng-Robinson Programs. Research Report No. RR-28, Gas Processors Association, Tulsa.

Perschke, D. R. 1988. *Equation of State Phase Behavior Modeling for Compositional Simulation*. PhD dissertation, University of Texas at Austin, Austin, Texas.

Perschke, D. R., Chang, Y.-B., Pope, G. A. et al. 1989. Comparison of Phase Behavior Algorithms for an Equation-of-State Compositional Simulator. SPE-19443-MS.

Shanno, D. F. 1970. Conditioning of Quasi-Newton Methods for Function Minimization. *Math. Comput.* **24** (111): 647–656. https://doi.org/10.2307/2004840.

Teh, Y. S. and Rangaiah, G. P. 2002. A Study of Equation-Solving and Gibbs Free Energy Minimization Methods for Phase Equilibrium Calculations. *Chem. Eng. Res. Des.* **80** (7): 745–759. https://doi.org/10.1205/026387602320776821.

Tessier, S. R., Brennecke, J. F., and Stadtherr, M. A. 2000. Reliable Phase Stability Analysis for Excess Gibbs Energy Models. *Chem. Eng. Sci.* **55** (10): 1785–1796. https://doi.org/10.1016/S0009-2509(99)00442-X.

Trangenstein, J. A. 1985. Minimization of Gibbs Free Energy in Compositional Reservoir Simulation. Presented at the SPE Reservoir Simulation Symposium, Dallas, 10–13 February. SPE-13520-MS. https://doi.org/10.2118/13520-MS.

Trangenstein, J. A. 1987. Customized Minimization Techniques for Phase Equilibrium Computations in Reservoir Simulation. *Chem. Eng. Sci.* **42** (12): 2847–2863. https://doi.org/10.1016/0009-2509(87)87051-3.

Venkataraman, S. and Lucia, A. 1986. Exploiting the Gibbs-Duhem Equation in Separation Calculations. *AIChE J.* **32** (7): 1057–1066. https://doi.org/10.1002/aic.690320702.

Venkataraman, S. and Lucia, A. 1987. Avoiding Variable-Scaling Problems Using the Gibbs-Helmholtz Equation. *Comput. Chem. Eng.* **11** (1): 73–76. https://doi.org/10.1016/0098-1354(87)80007-8.

Whitson, C. H. and Michelsen, M. L. 1989. The Negative Flash. *Fluid Phase Equilibr.* **53:** 51–71. https://doi.org/10.1016/0378-3812(89)80072-X.

Wilson, G. 1969. A Modified Redlich-Kwong Equation of State, Application to General Physical Data Claculations. Paper presented at AIChE 65th National Meeting, Cleveland, Ohio, USA, 4–7 May.

Xu, G., Brennecke, J. F., and Stadtherr, M. A. 2002. Reliable Computation of Phase Stability and Equilibrium from the SAFT Equation of State. *Ind. Eng. Chem. Res.* **41** (5): 938–952. https://doi.org/10.1021/ie0101801.

Xu, G., Haynes, W. D., and Stadtherr, M. A. 2005. Reliable Phase Stability Analysis for Asymmetric Models. *Fluid Phase Equilibr.* **235** (2): 152–165. https://doi.org/10.1016/j.fluid.2005.06.016.

Xu, G., Scurto, A. M., Castier, M. et al. 2000. Reliable Computation of High-Pressure Solid-Fluid Equilibrium. *Ind. Eng. Chem. Res.* **39** (6): 1624–1636. https://doi.org/10.1021/ie990653s.

Zhu, D. and Okuno, R. 2015. Robust Isenthalpic Flash for Multiphase Water/Hydrocarbon Mixtures. *SPE J.* **20** (6): 1350–1365. SPE-170092-PA. https://doi.org/10.2118/170092-PA.

Zhu, D. and Okuno, R. 2016. Multiphase Isenthalpic Flash Integrated with Stability Analysis. *Fluid Phase Equilibr.* **423** (15 September): 203–219. https://doi.org/10.1016/j.fluid.2016.04.005.

Zhu, D., Shekhar, C., and Okuno, R. 2017. Tangent-Plane Algorithm for Multiphase Flash Integrated with Stability Analysis; software package.

Appendix A—Formulation for Global Minimization of the Gibbs Free Energy

The correct phase equilibrium for a given pressure (P), temperature (T), and overall composition $\underline{z}$ is defined by x_{ij} ($i = 1, 2, \ldots, N_C$ and $j = 1, 2, \ldots, N_P$) that gives the global minimum of

$$\underline{G}_R = \sum_{j=1}^{N_P} \sum_{i=1}^{N_C} \beta_j x_{ij} \ln(x_{ij}\varphi_{ij}), \quad \text{(A-1)}$$

where x_{ij} is the mole fraction of component i in phase j, β_j is the mole fraction of phase j, φ_{ij} is the fugacity coefficient of component i in phase j, N_C is the number of components, and N_P is the number of equilibrium phases. The following constraints are to be satisfied:

$$z_i = \sum_{j=1}^{N_P} \beta_j x_{ij}, \quad \ldots\ldots (A\text{-}2)$$

$$\sum_{j=1}^{N_P} \beta_j = 1.0, \quad \ldots\ldots (A\text{-}3)$$

$$\sum_{i=1}^{N_C} x_{ij} = 1.0, \quad \ldots\ldots (A\text{-}4)$$

where $\beta_j \geq 0$ and $x_{ij} \geq 0$ for $i = 1, 2, \ldots, N_C$ and $j = 1, 2, \ldots, N_P$.

The tangent plane (T) to the Gibbs free energy at composition $\underline{x}^0$ can be derived by the first-order Taylor-series expansion of the Gibbs free energy around $\underline{x}^0$ (Okuno 2009):

$$T(\underline{x}) = \underline{G}(\underline{x}^0) + \sum_{i=1}^{N_C} (x_i - x_i^0) \frac{\partial \underline{G}(\underline{x})}{\partial x_i}\bigg|_{\underline{x}=\underline{x}^0} = \underline{G}(\underline{x}^0) + \sum_{i=1}^{N_C} x_i \overline{G}_i(\underline{x}^0) - \sum_{i=1}^{N_C} x_i^0 \overline{G}_i(\underline{x}^0) = \sum_{i=1}^{N_C} x_i \overline{G}_i(\underline{x}^0). \quad \ldots\ldots (A\text{-}5)$$

Note that the plane T spans composition space; i.e., $T = T(\underline{x})$. Then, the TPD function (D), which also spans composition space, is derived by subtracting T from the Gibbs free energy. That is,

$$D(\underline{x}) = G(\underline{x}) - T(\underline{x}) = \sum_{i=1}^{N_C} x_i [\overline{G}_i(\underline{x}) - \overline{G}_i(\underline{x}^0)], \quad \ldots\ldots (A\text{-}6)$$

or in dimensionless form,

$$D_R(\underline{x}) = D(\underline{x})/RT = \sum_{i=1}^{N_C} x_i [\ln x_i \varphi_i(\underline{x}) - \ln x_i^0 \varphi_i(\underline{x}^0)]. \quad \ldots\ldots (A\text{-}7)$$

At a stationary point of $D(\underline{x})$, the first-order derivatives are all zero; that is,

$$\partial D(\underline{x})/\partial x_i = [\overline{G}_i(\underline{x}) - \overline{G}_i(\underline{x}^0)] - [\overline{G}_{N_C}(\underline{x}) - \overline{G}_{N_C}(\underline{x}^0)] = 0, \quad \ldots\ldots (A\text{-}8)$$

or

$$[\overline{G}_i(\underline{x}) - \overline{G}_i(\underline{x}^0)] = [\overline{G}_{N_C}(\underline{x}) - \overline{G}_{N_C}(\underline{x}^0)], \quad \ldots\ldots (A\text{-}9)$$

for $i = 1, 2, \ldots, (N_C - 1)$. Therefore, $D(\underline{x})$ at a stationary point can be expressed as

$$D(\underline{x}) = \sum_{i=1}^{N_C} x_i [\overline{G}_{N_C}(\underline{x}) - \overline{G}_{N_C}(\underline{x}^0)] = \overline{G}_{N_C}(\underline{x}) - \overline{G}_{N_C}(\underline{x}^0) = \overline{G}_i(\underline{x}) - \overline{G}_i(\underline{x}^0), \quad \ldots\ldots (A\text{-}10)$$

or in dimensionless form,

$$D_R(\underline{x}) = \ln x_i \varphi_i(\underline{x}) - \ln x_i^0 \varphi_i(\underline{x}^0) \quad \ldots\ldots (A\text{-}11)$$

for $i = 1, 2, \ldots, N_C$.

Rearrangement of Eq. A-11 yields the traditional stationarity equation of Michelsen (1982a):

$$\ln[X_i \varphi_i(\underline{x})] - \ln[x_i^0 \varphi_i(\underline{x}^0)] = 0, \quad \ldots\ldots (A\text{-}12)$$

where $X_i = x_i \exp(-D/RT) = x_i \exp(-D_R)$, and $i = 1, 2, \ldots, N_C$. Eq. A-12 has been widely used to search for a stationary point of D_R in the stationary-point method of phase-stability analysis (Michelsen 1982a), as part of the conventional sequential phase-stability and -split calculation. In the stationary-point method, $\underline{x}^0$ is set to $\underline{z}$ for testing the stability of the overall composition $\underline{z}$. For testing the stability of a multiphase system, $\underline{x}^0$ is set to one of the equilibrium phases under consideration. Note again that Eqs. A-8 through A-12 hold only when $\underline{x}$ corresponds to a stationary point of D_R.

Eq. A-12 reduces to the fugacity equations for N_P stationary points that are on the tangent plane T (i.e., N_P equilibrium phase compositions, at which $D_R = 0$). At all other stationary points, D_R should be positive because the T plane cannot lie above the G surface at any composition at an equilibrium state (Baker et al. 1982). Hence,

$$D_{Rj} = \sum_{i=1}^{N_C} x_{ij} (\ln x_{ij} \varphi_{ij} - \ln x_{ir} \varphi_{ir}) \geq 0, \quad \ldots\ldots (A\text{-}13)$$

for $j = 1, 2, \ldots, N_S$ at a specified T and P. N_S is the number of stationary points of the dimensionless TPD function, D_R, defined with a reference equilibrium phase composition (x_{ir}, where $i = 1, 2, \ldots, N_C$). Note that $N_S = N_P + N_U$, where N_U is the number of stationary points that are not equilibrium phases (i.e., N_U stationary points at which $D_R > 0$). Eq. A-13 can be also written as

$$D_{Rj} = \ln x_{ij} \varphi_{ij} - \ln x_{ir} \varphi_{ir} \geq 0, \quad \ldots\ldots (A\text{-}14)$$

when $\underline{x}_j$ ($j = 1, 2, \ldots, N_S$) are all stationary points.

The unified formulation for phase-stability and -split calculation in the current paper is to find a set of x_{ij} ($i = 1, 2, \ldots, N_C$, and $j = 1, 2, \ldots, N_S$) such that $D_{Rj} = 0$ subject to Eqs. A-2, A-3, and A-4 for equilibrium phases $j = 1, 2, \ldots, N_P$, and $D_{Rj} > 0$ subject to Eq. A-4 for the other stationary points that are not equilibrium phases $j = (N_P+1), (N_P+2)\ldots, N_S$. The algorithm presented in the current paper uses the D_R function with adaptive selection of the reference composition $\underline{x}_r$ for an arbitrary number of iterative compositions, which converge to stationary points with TPDs D_{Rj}.

Appendix B—Flow Chart for the Algorithm Developed in This Research

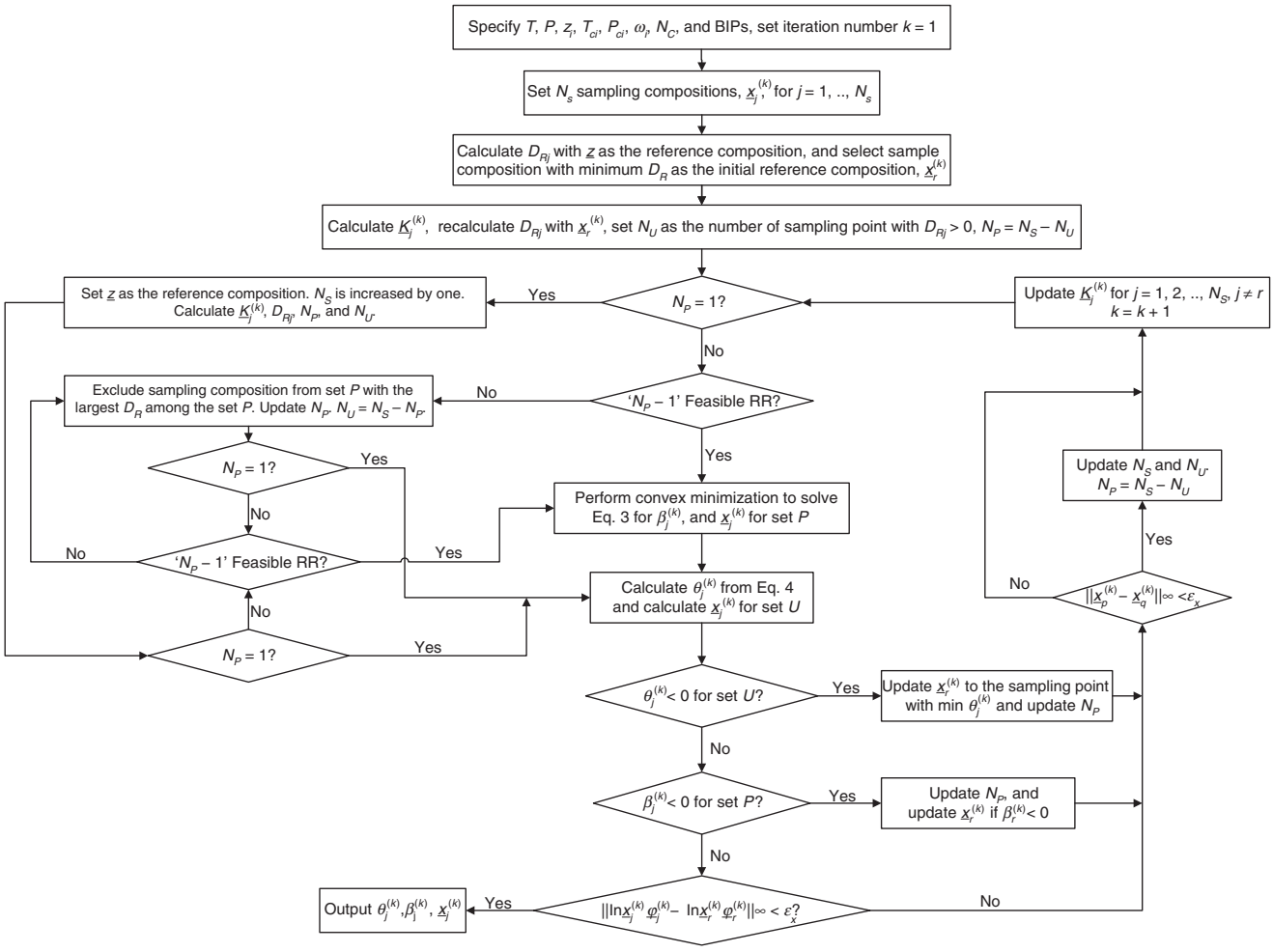

Appendix C—Initialization of Sampling Compositions Used in This Paper

The algorithm developed in this research attempts to find stationary points of TPD that give the global minimum of the Gibbs free energy for the fluid under consideration with a specified $\underline{z}$, P, and T. One of the most important factors that affect global convergence of the algorithm is how iterative sampling compositions are distributed in composition space. If no reliable information is available regarding equilibrium phase compositions for the fluid of interest at specified conditions, sampling compositions should be distributed in composition space in a certain systematic manner. Ideally, they are expected to find all stationary points of TPD. Such a possibility is generally expected to increase as more sampling compositions are used, unless they are placed close to each other.

Here, we present the procedure used in this paper to distribute sampling compositions uniformly with respect to the specified $\underline{z}$, for the initialization of the algorithm developed. First, N_C sampling compositions are placed near the N_C vertices of composition space. If more sampling compositions are desired, the composition space is divided into N_C different regions that have the overall composition $\underline{z}$ as the common vertex. Each of the N_C regions is defined by this common vertex z and the other (N_C–1) vertices among N_C vertices of pure components. Then, a systematic procedure is applied to distribute sampling compositions around the central point for each of the N_C regions. The number of sampling compositions placed in each region can be defined individually, or correlated with the relative size of that region to the entire composition space, as described later. A stepwise description is given here.

Step 1. Distribute N_C sampling compositions near the N_C vertices of composition space (e.g., 99.9% that component and 0.1% the equimolar mixture of the other components).

Step 2. If more sampling compositions are desired, the composition space is divided into N_C different regions (R_i for $i = 1, 2,\ldots, N_C$) that have the overall composition $\underline{z}$ as the common vertex. Each of the N_C regions is defined by $\underline{z}$ and the other (N_C–1) vertices among N_C vertices of pure components. Then, define the number of sampling compositions $N_{Si} \geq 1$ ($i = 1, 2,\ldots N_C$) for R_i ($i = 1, 2,\ldots, N_C$). Set $i = 1$.

Step 3. For the ith region R_i, calculate the arithmetic mean of the N_C compositions, $\underline{z}$ and (N_C–1) pure components. This corresponds to the central point in R_i, and becomes a sampling composition. Then, connect the central point with the N_C vertices of R_i. This results in N_C lines in R_i.

Step 4. For R_i, evenly divide each of the N_C lines obtained from Step 3 into r_{1i} segments ($r_{1i} \geq 1$). This results in $(r_{1i}-1)N_C$ sampling compositions within R_i.

Step 5. If $r_{1i} \geq 2$, construct $(r_{1i}-1)N_C(N_C-1)/2$ lines that are parallel to edges of composition space by connecting sampling compositions obtained from Step 4.

Step 6. Evenly divide the $(r_{1i}-1)N_C(N_C-1)/2$ lines obtained from Step 5 into r_{2i} segments ($r_{2i} \geq 1$). This results in $(r_{1i}-1)(r_{2i}-1)N_C(N_C-1)/2$ sampling compositions within R_i.

Step 7. Repeat Steps 3 through 6 for the next region until sampling compositions are distributed for all N_C regions defined in Step 2. That is, increase i by one, where $i \leq N_C$. Go back to Step 3.

The first step gives N_C sampling compositions. Step 3 gives one sampling composition at the center for each region; hence, N_C sampling compositions in the N_C regions. Steps 4 and 6 give $(r_{1i}-1)N_C$ and $(r_{1i}-1)(r_{2i}-1)N_C(N_C-1)/2$ sampling compositions, respectively, for each region. Therefore, the total number of sampling compositions distributed by use of the procedure given above is $N_C+\Sigma_i[1+(r_{1i}-1)N_C+(r_{1i}-1)(r_{2i}-1)N_C(N_C-1)/2]$ for $N_C \geq 2$. The minimum N_S is $2N_C$ ($N_C \geq 2$) when $r_1 = 1$ for all regions; i.e., N_C compositions from Steps 1 and 3.

In Step 2, N_{Si} (≥ 1) for R_i ($i = 1, 2, \ldots, N_C$) can be correlated with the size of R_i relative to the entire composition space as follows.

Step 2-1. Calculate $n_{Si} = \left(z_i^n \Big/ \sum_{i=1}^{N_C} z_i^n\right)(N_{S\max} - N_C)$, where $N_{S\max}$ is the maximum number of initial sampling compositions specified by the user. The exponent n can be also specified.

Step 2-2. Solve $n_{Si} = (r_1-1)N_C+(r_1-1)(r_2-1)N_C(N_C-1)/2$ for r_1 and r_2 subject to a certain constraint regarding r_1 and/or r_2, such as $r_2 = r_1-1$, which is used in this paper.

Step 2-3. Round down r_1 and r_2 to make them integers, r_{1i} and r_{2i}. Calculate $N_{Si} = 1+(r_{1i}-1)N_C+(r_{1i}-1)(r_{2i}-1)N_C(N_C-1)/2$. Note that $N_S = N_C+\sum_{i=1}^{N_C} N_{Si} \leq N_{S\max}$ because of the rounding of r_1 and r_2.

As an example, **Fig. C-1** shows the sampling compositions distributed by use of the previously discussed procedure (Steps 1 through 7) for $N_C = 3$, $N_{S\max} = 100$, and $n = 1$ along with the constraint $r_2 = r_1-1$. The resulting N_S is 81, which consists of three compositions near the pure components, three at the centers of three regions, and 75 in the largest region defined by $\underline{z}$ and Components 2 and 3.

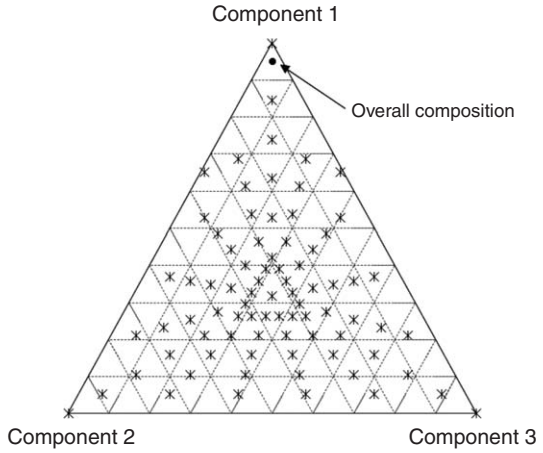

Fig. C-1—Sampling compositions distributed for $N_C = 3$ by use of the procedure given in Appendix C. The resulting N_S is 81 with $N_{S\max} = 100$, $n = 1.0$, and the constraint $r_2 = r_1-1$.

This is merely one of many possible procedures to systematically distribute sampling compositions; it is not the purpose of Appendix C to single out a procedure that yields rapid convergence of the algorithm. When reasonable estimates are available for potential phase compositions, they can be used to initialize the algorithm.

Appendix D—Movement of Sampling Compositions for Cases 1 and 2

Here, we show how sampling compositions move in composition space during the iteration with the new algorithm for Cases 1 and 2. The EOS parameters and solutions for these cases were discussed in the Case Studies section.

Case 1. Case 1 was a ternary mixture consisting of H_2O, C_3, and n-C_{16} at 560 K and 65 bar (Tables 1 and 2). The convergence behavior of the new algorithm was presented in Fig. 4. **Fig. D-1** shows the movement of sampling compositions at selected iteration steps. In Fig. D-1, a star represents the overall composition. Solid squares represent the sampling compositions in set U. The reference composition in set P is shown by a solid diamond, and the other sampling compositions in set P are hollow squares. This symbolic notation is used throughout this appendix.

After the initialization, six sampling compositions are distributed in composition space, in which three are near compositional vertices and the other three are in the central points of each area, as can be seen in Fig. D-1a. All six sampling compositions are updated significantly after the first iteration, where three sampling compositions are set U with positive θ values. Figs. D-1b and D-1c show that the six compositions do not merge (i.e., N_S remains six) during the second and third iterations, but the reference composition is adaptively selected on the basis of Step 7 of the new algorithm. That is, the composition with negative θ value is selected as the reference composition during the iterations.

After the fourth iteration, a composition in set U merges into a composition in set P, resulting in $N_P = 5$ and $N_U = 0$ (Fig. D-1e). The reference composition used from iteration step 4 until the final convergence is in the vicinity of the equilibrium L_1 phase. Two compositions merge during iteration step 5, which gives $N_S = 3$. The correct $N_S = 2$ (i.e., $N_P = 2$ and $N_U = 0$) is identified at the seventh iteration. As can be seen in Figs. D-1g and D-1h, the compositions in set P at the seventh iteration are in the vicinity of the final equilibrium compositions. The converged compositions in set P are connected by the tie line in Fig. D-1h.

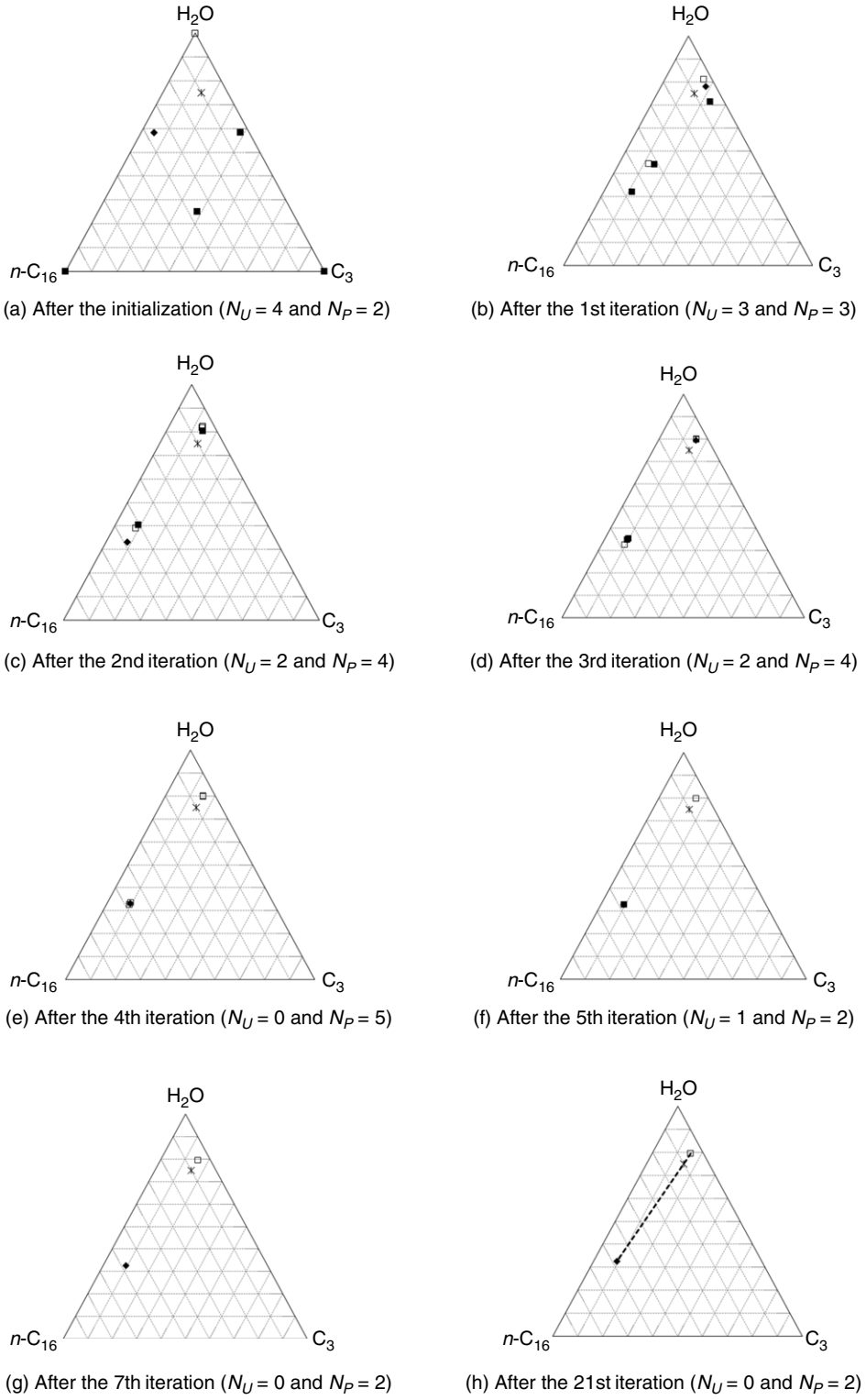

(a) After the initialization ($N_U = 4$ and $N_P = 2$)

(b) After the 1st iteration ($N_U = 3$ and $N_P = 3$)

(c) After the 2nd iteration ($N_U = 2$ and $N_P = 4$)

(d) After the 3rd iteration ($N_U = 2$ and $N_P = 4$)

(e) After the 4th iteration ($N_U = 0$ and $N_P = 5$)

(f) After the 5th iteration ($N_U = 1$ and $N_P = 2$)

(g) After the 7th iteration ($N_U = 0$ and $N_P = 2$)

(h) After the 21st iteration ($N_U = 0$ and $N_P = 2$)

Fig. D-1—Movement of sampling compositions for Case 1. A star represents the overall composition. Solid squares represent the sampling compositions in set *U*. The reference composition in set *P* is shown by a solid diamond, and the other sampling compositions in set *P* are hollow squares. (a) After the initialization ($N_U = 4$ and $N_P = 2$); (b) after the first iteration ($N_U = 3$ and $N_P = 3$); (c) after the second iteration ($N_U = 2$ and $N_P = 4$); (d) after the third iteration ($N_U = 2$ and $N_P = 4$); (e) after the fourth iteration ($N_U = 0$ and $N_P = 5$); (f) after the fifth iteration ($N_U = 1$ and $N_P = 2$); (g) after the seventh iteration ($N_U = 0$ and $N_P = 2$); (h) after the 21st iteration ($N_U = 0$ and $N_P = 2$).

Fig. D-2 shows the motion of the sampling compositions by use of a triangular prism, where each horizontal cross section represents the ternary diagram at a certain iteration step. The same iteration steps as Fig. D-1 are presented. The merging of sampling compositions can be seen at the fourth, fifth, and seventh iteration steps.

Case 2. Fig. D-3 presents the motion of sampling compositions for the binary mixture consisting of 97% C_1 and 3% H_2S at 190 K and 40.53 bar (Tables 3 and 4). The convergence behavior was presented in Fig. 6.

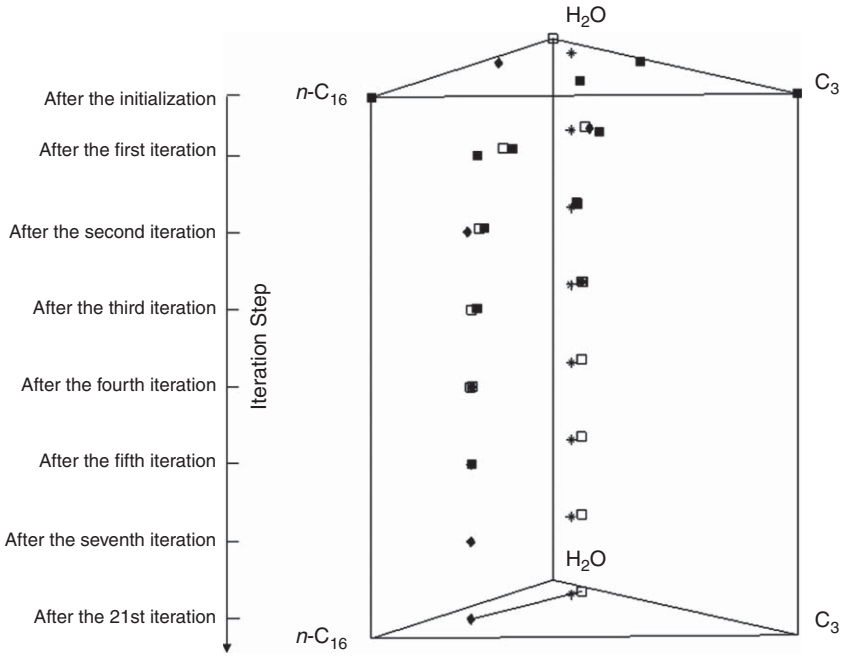

Fig. D-2—Triangular prism to present sampling compositions at selected iteration steps for Case 1.

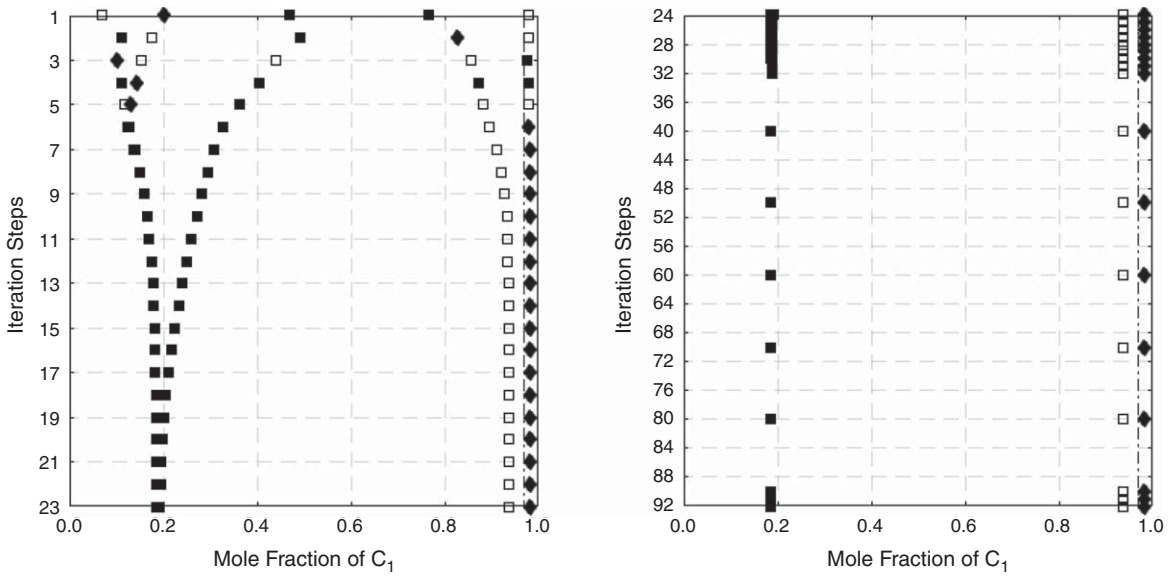

(a) Iteration steps from 1 through 23

(b) Iteration steps from 24 through 92

Fig. D-3—Movement of sampling compositions for Case 2. (a) Iteration Steps 1 through 23; (b) Iteration Steps 24 through 92.

$N_S = 5$ is identified after initialization. Early in the iteration, compositions often switch between sets P and U while smoothly changing their compositions. From the seventh iteration on, the compositions in set U move toward the L_1-like composition (the left lobe in Fig. 5). The number of sampling compositions in set U, N_U, reduces from three to two to one at iteration steps 7, 10, and 31, respectively. From the 31st iteration on, the correct $N_S = 3$ ($N_P = 2$ and $N_U = 1$) is maintained until the final convergence at the 92nd iteration.

Di Zhu is a PhD degree candidate in petroleum engineering in the Department of Petroleum and Geosystems Engineering at the University of Texas at Austin. Her research interests include multiphase behavior for complex reservoir fluids, miscible displacement, and numerical reservoir simulation. Zhu holds a bachelor's degree from Yangtze University, China, and a master's degree from the China University of Petroleum (East China), both in geodetection and information technology. She is a member of SPE.

Sara Eghbali is a PhD degree candidate in petroleum engineering at the University of Alberta. She has 2 years of industrial experience as a reservoir engineer with Tehran Energy Consultant Company, Iran. Eghbali's research interests include phase behavior, reservoir characterization, and reservoir simulation. She holds bachelor's and master's degrees in petroleum engineering, both from Sharif University of Technology, Iran. Eghbali is a member of SPE.

Chandra Shekhar is a master's degree student in the Department of Petroleum and Geosystems Engineering at the University of Texas at Austin. He has 2 years of industrial experience as a process engineer with KBR. Shekhar's research interests include modeling of multiphase behavior, numerical reservoir simulation, and enhanced oil recovery. He holds a bachelor's degree in chemical engineering from the Indian Institute of Technology. Shekhar is a member of SPE.

Ryosuke Okuno is an assistant professor in the Department of Petroleum and Geosystems Engineering at the University of Texas at Austin and holds the Pioneer Corporation Faculty Fellowship in Petroleum Engineering at the University of Texas at Austin. Before his current position, he served as an assistant professor of petroleum engineering at the University of Alberta from 2010 to 2015. Okuno also has 7 years of industrial experience as a reservoir engineer with Japan Petroleum Exploration Company Limited and is a registered professional engineer in Alberta, Canada. His research and teaching interests include enhanced oil recovery, heavy-oil recovery, unconventional resources, numerical reservoir simulation, thermodynamics, multiphase behavior, and applied mathematics. Okuno holds bachelor's and master's degrees in geosystems engineering from the University of Tokyo, and a PhD degree in petroleum engineering from the University of Texas at Austin. He is a member of SPE, a recipient of the 2012 SPE Petroleum Engineering Junior Faculty Research Initiation Award, and an associate editor for *SPE Journal*.